NASA TN D-156

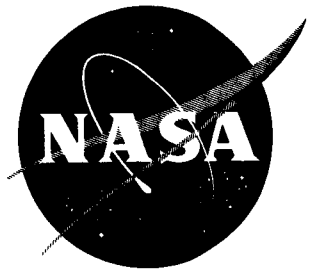

TECHNICAL NOTE
D-156

ANALYTICAL INVESTIGATION OF EFFECT OF SPIN ENTRY TECHNIQUE ON SPIN AND RECOVERY CHARACTERISTICS FOR A 60° DELTA-WING AIRPLANE

By Stanley H. Scher, Ernie L. Anglin,
and George F. Lawrence

Langley Research Center
Langley Field, Va.

NATIONAL AERONAUTICS AND SPACE ADMINISTRATION

WASHINGTON December 1959

NATIONAL AERONAUTICS AND SPACE ADMINISTRATION

TECHNICAL NOTE D-156

ANALYTICAL INVESTIGATION OF EFFECT OF SPIN ENTRY TECHNIQUE ON SPIN AND RECOVERY CHARACTERISTICS FOR A 60° DELTA-WING AIRPLANE

By Stanley H. Scher, Ernie L. Anglin,
and George F. Lawrence

SUMMARY

A high-speed digital computer study has been made to investigate analytically the effects of differences in full-scale-airplane and spin-tunnel-model testing technique on spins and recoveries obtained for a configuration representative of a current 60° delta-wing fighter-type airplane. Calculations were made to simulate airplane spin entry starting from trimmed level flight and to simulate an airplane spin with the use of the spin-tunnel entry technique which starts the motion at a high angle of attack with rotation applied. Six-degree-of-freedom equations of motion and available data for nonlinear aerodynamic stability derivatives were used.

Results obtained for the design investigated indicate that the method by which a spin is entered may in some instances lead to significant differences in spins and recoveries. The investigation revealed that different spins may be obtainable from an entry from trimmed level flight and from an entry with applied rotation similar to the method used in testing of a spin-tunnel model. Any difference in results, however, may be dependent upon the directional characteristics of the airplane at spinning attitudes, and this difference could, in turn, be influenced by Reynolds number. Factors contributing to possible differences in spins and recoveries are the different aerodynamic and inertia moments acting during the two types of spin-entry maneuvers, the effects of air density, and the effects of variation of air density with altitude.

The results of the investigation emphasize that, as indicated by spin research of the past few years at Langley Research Center, proper evaluation of full-scale spin and recovery characteristics of modern designs from spin-tunnel tests requires cognizance of both tunnel technique and Reynolds number.

INTRODUCTION

In reference 1, it was reported that free-spinning-tunnel tests of models, properly interpreted, can give good indications of the probable spin and recovery characteristics of corresponding airplanes. Reference 1 also points out that significant differences may sometimes be likely between model and airplane results, a likelihood which has become more pronounced with current high-speed designs. These differences can be due to such factors as possible aerodynamic scale effects and variations in testing techniques between airplanes and free-spinning-tunnel models. These variations in testing techniques refer to the manner in which spins are achieved in flight and in a free-spinning tunnel. In flight, an airplane enters an incipient spin following roll-off or a yawing divergence at an angle of attack just above the stalling angle of attack. Unless proper control manipulation is applied to stop the incipient spin, it will usually develop fully to an equilibrium spinning condition within about two to five turns after the incipient spin is initiated. In spin-tunnel testing technique, a model is hand-launched into the vertical airstream of the tunnel with rotation applied at a very high angle of attack (80° to 90°) above the stall. From this initial attitude, the model may adjust the angle of attack and rotation rate and achieve equilibrium in a developed spin.

The primary purpose of the present investigation is to determine analytically the differences in spin and recovery characteristics which might be indicated for a current fighter-airplane configuration as a result of differences in spin-tunnel and flight testing methods. According to information furnished Langley Research Center by the Air Force, there were some significant differences between the spin-tunnel-model results and the full-scale airplane flight-test results for the 60° delta-wing fighter configuration which was selected for use in this investigation. In addition, there was available a relatively large amount of aerodynamic-stability-derivative data considered applicable for this configuration (ref. 2).

Six-degree-of-freedom equations of motion were solved with the use of a high-speed digital computer in calculations which simulated both flight and spin-tunnel testing techniques. Results in the form of time histories of some of the attitude and angular-velocity variables of the spinning motions are presented, and comparisons of the calculated spins and recoveries are made with full-scale and spin-tunnel-model results.

SYMBOLS

The body system of axes is used. This system of axes, related angles, and positive directions of corresponding forces and moments are illustrated in figure 1.

C_X longitudinal-force coefficient, $\frac{F_X}{\frac{1}{2}\rho V_R^2 S}$

C_Y side-force coefficient, $\frac{F_Y}{\frac{1}{2}\rho V_R^2 S}$

C_Z normal-force coefficient, $\frac{F_Z}{\frac{1}{2}\rho V_R^2 S}$

C_l rolling-moment coefficient, $\frac{M_X}{\frac{1}{2}\rho V_R^2 Sb}$

C_m pitching-moment coefficient, $\frac{M_Y}{\frac{1}{2}\rho V_R^2 S\bar{c}}$

C_n yawing-moment coefficient, $\frac{M_Z}{\frac{1}{2}\rho V_R^2 Sb}$

F_X longitudinal force acting along X body axis, lb

F_Y lateral force acting along Y body axis, lb

F_Z normal force acting along Z body axis, lb

M_X rolling moment acting about X body axis, ft-lb

M_Y pitching moment acting about Y body axis, ft-lb

M_Z yawing moment acting about Z body axis, ft-lb

W weight, lb

S	wing area, sq ft
b	wing span, ft
ρ	air density, slugs/cu ft
V	vertical component of velocity of airplane center of gravity (rate of descent), ft/sec
V_R	resultant linear velocity, ft/sec
u,v,w	components of resultant velocity V_R along X, Y, and Z body axes, respectively, ft/sec
Ω	resultant angular velocity, radians/sec (or rps where noted)
p,q,r	components of resultant angular velocity Ω about X, Y, and Z body axes, respectively, radians/sec
m	mass of airplane, $\frac{W}{g}$, slugs
$\bar{c}$	mean aerodynamic chord, ft
I_X,I_Y,I_Z	moments of inertia about X, Y, and Z body axes, respectively, slug-ft^2
I_{XZ}	product of inertia in XZ-plane, positive when principal axis is inclined below reference line at nose, slug-ft^2
$\frac{I_X - I_Y}{mb^2}$	inertia yawing-moment parameter
$\frac{I_Y - I_Z}{mb^2}$	inertia rolling-moment parameter
$\frac{I_Z - I_X}{mb^2}$	inertia pitching-moment parameter
g	acceleration due to gravity, taken as 32.17 ft/sec^2
h_1	altitude at beginning of time increment, ft
h_2	altitude at end of time increment, ft

Δt time increment, sec

α angle of attack, angle between relative wind V_R projected into XZ-plane of symmetry and X body axis, positive when relative wind comes from below XY body plane, deg

β angle of sideslip, angle between relative wind V_R and projection of relative wind on XZ-plane, positive when relative wind comes from right of plane of symmetry, deg

δ_e elevator deflection with respect to fuselage reference line, positive with trailing edge down, deg

δ_r rudder deflection with respect to fin, positive with trailing edge to left, deg

δ_a aileron deflection with respect to chord line of wing, positive with trailing edge of right aileron down, deg

ϕ angle between Y body axis and horizontal measured in vertical plane, positive for erect spins when right wing downward and for inverted spins when left wing downward, deg

ϕ_e total angular movement of Y body axis from horizontal plane measured in YZ body plane, positive when clockwise as viewed from rear of airplane (if X body axis is vertical, ϕ_e is measured from a reference position in horizontal plane), radians

θ_e total angular movement of X body axis from horizontal plane measured in vertical plane, positive when airplane nose is above horizontal plane, radians or deg

ψ_e horizontal component of total angular deflection of X body axis from reference position in horizontal plane, positive when clockwise as viewed from vertically above airplane, radians

$$C_{l_p} = \frac{\partial C_l}{\partial\left(\frac{pb}{2V_R}\right)}$$

$$C_{n_p} = \frac{\partial C_n}{\partial\left(\frac{pb}{2V_R}\right)}$$

$$C_{l_r} = \frac{\partial C_l}{\partial\left(\frac{rb}{2V_R}\right)}$$

$$C_{n_r} = \frac{\partial C_n}{\partial\left(\frac{rb}{2V_R}\right)}$$

$$C_{m_q} = \frac{\partial C_m}{\partial\left(\frac{q\bar{c}}{2V_R}\right)}$$

$$C_{m_{\dot{\alpha}}} = \frac{\partial C_m}{\partial\left(\frac{\dot{\alpha}\bar{c}}{2V_R}\right)}$$

$$C_{n_{\dot{\beta}}} = \frac{\partial C_n}{\partial\left(\frac{\dot{\beta}b}{2V_R}\right)}$$

$$C_{l_\beta} = \frac{\partial C_l}{\partial\beta}$$

$$C_{n_\beta} = \frac{\partial C_n}{\partial\beta}$$

$$C_{Y_\beta} = \frac{\partial C_Y}{\partial\beta}$$

$\Delta C_{m,e}$ incremental pitching-moment coefficient due to elevator deflection

$\Delta C_{Z,e}$ incremental normal-force coefficient due to elevator deflection

$\Delta C_{X,e}$ incremental longitudinal-force coefficient due to elevator deflection

$\Delta C_{n,r}$ incremental yawing-moment coefficient due to rudder deflection

$\Delta C_{Y,r}$ incremental side-force coefficient due to rudder deflection

$\Delta C_{l,r}$ incremental rolling-moment coefficient due to rudder deflection

$\Delta C_{l,a}$ incremental rolling-moment coefficient due to aileron deflection

$\Delta C_{n,a}$ incremental yawing-moment coefficient due to aileron deflection

$\Delta C_{Y,a}$ incremental side-force coefficient due to aileron deflection

A dot over a symbol represents a derivative with respect to time, for example, $\dot{u} = \frac{du}{dt}$.

ANALYSIS, METHODS, AND CALCULATIONS

Spin studies of a 60° delta-wing fighter-type airplane have been conducted both in an Air Force spin tunnel at Wright Air Development Center and in flight. The model spun at a higher angle of attack and at a considerably more rapid rate of rotation than did the corresponding airplane as may be seen from the following table of average values:

	α, deg	Ω, rps	Turns for recovery
Airplane	75	0.16	$1\frac{2}{3}$
Model (full-scale values)	85	0.36	∞

Differences between model and airplane results due to such factors as variations in spin entry technique between airplanes and models and also to possible aerodynamic scale effects, that is, Reynolds number, can sometimes be anticipated, particularly for modern long-nose designs loaded heavily along the fuselage. One of the primary effects of Reynolds number appears to be a large change in the nature of the flow over the elongated nose portion of the fuselage of modern fighter configurations, which can change the magnitude and/or direction of the yawing moment acting during spins (refs. 1 and 3). For the configuration considered in the present investigation, the forward part of the fuselage is nearly circular in cross section, but from the windshield location back to the wing leading edge, the fuselage cross section varies considerably due

to air intakes and other design details. No significant effect of Reynolds number variations on the yawing moment appears to be expected on the circular portion of the nose, but some effects possibly could be expected on the rest of the nose (ref. 4).

The calculation of motions for the present investigation were made with the use of a high-speed automatic digital computer which solved the equations of motion and associated formulas listed in the APPENDIX. The equations of motion are Euler's equations representing six degrees of freedom along and about the airplane body system of axes. (See fig. 1 for illustration of body axes.) The mass and dimensional characteristics used in the calculations are those for the full-scale airplane and are listed in table I. A three-view sketch of the general shape of the configuration is shown in figure 2. Most of the aerodynamic-derivative data were nonlinear and are presented in the plots shown in figures 3 to 9. Most of these data were obtained from the results presented in reference 2. The cross-rotary lateral aerodynamic stability derivatives in figure 6 were taken from applicable results of unpublished wind-tunnel tests made for a similar 60° delta-wing model. The data in figures 3 to 9 were obtained for a Reynolds number of about 9.0×10^5 based on the mean aerodynamic chord of the delta-wing model, and about 2.0×10^5 based on an average vertical depth of the model fuselage nose section. Values of the derivatives C_{m_q} and $C_{m_{\dot{\alpha}}}$ used in the pitching equation of motion (given in APPENDIX) were not obtained from wind-tunnel measurements, and each was arbitrarily varied from zero to -0.9 in the investigation.

L 2 1 8

The rotary lateral derivatives presented in figures 5 and 6 were actually obtained as combination lateral derivatives which include the effects of $\dot{\beta}$. (For example, C_{n_r} is actually $C_{n_r} - C_{n_{\dot{\beta}}} \cos \alpha$.) Inasmuch as the full derivatives could not be separated into their component parts, it was arbitrarily decided for this investigation to treat the derivatives as though they were due to angular velocities about body axes. The oscillation frequency for the tests from which the derivatives in figure 5 were obtained was about 1 cps, whereas the derivatives in figure 6 were average values corresponding to a test frequency of about 0.6 cps. Obviously, any effects which frequency of the oscillations may have on these derivatives are neglected in the present calculations.

The calculations were made to simulate attempted spin entries from a condition of trimmed level flight similar to that of the airplane and to simulate a condition under which a model is launched into a spin tunnel. (See table II.) For the calculations which simulated an entry from trimmed flight, the effect of the variation of air

density with altitude was included. For the calculations which simulated the spin-tunnel entry technique, air density was maintained constant as it is normally in a free-spinning tunnel, and representative values of attitude and rate of rotation were selected. For the present investigation, thrust and gyroscopic effects of the engine were neglected.

In order to start a calculation simulating an attempted spin entry from trimmed flight, the effects of deflecting the airplane elevator full up from its position for trimmed level flight were introduced as step-function machine inputs at zero time. As the motion developed, the time histories were monitored, and the computer was stopped momentarily to apply rudder and aileron controls at a time conducive to sustain the spin. For the calculations simulating spin-tunnel launchings, all controls were set at zero time to aid in obtaining a spin. For attempted recoveries from spins obtained after either type of entry, the controls were moved as desired. For the present investigation, the computing machine programming method allowed for calculated results accurate to three significant figures. Although this accuracy was considered greater than that required in the investigation, an analysis indicated that no appreciable saving in machine time could have been realized by decreasing the accuracy.

The significance of motions obtained in the calculations following application of controls for attempted recoveries were evaluated in a manner similar to that utilized in reference 1. In general, an airplane is considered to have recovered from the spin when the angle of attack at the center of gravity is below the stall. Usually, when this attitude is achieved, the airplane enters a steep pull-out dive without rotation. In some cases, however, the aircraft may be turning or rolling in a spiral glide or an aileron roll. Sometimes the airplane may roll or pitch to an inverted attitude from the erect spin and may still have some rotation, but this is also considered to be a recovery from the original erect spin.

RESULTS AND DISCUSSION

The results of the calculations are presented in the time-history plots of figures 10 to 18. In order to simplify presentation of the results, only a few pertinent variables of the motions are presented although time histories of all the attitude, velocity, and acceleration variables in the equations of motion were calculated. In figures 10 to 18, the plots presented are angle of attack α, angle of wing tilt ϕ, resultant angular velocity Ω, control-surface positions, and spinning turns completed with respect to time. In figures 10 and 11, yawing velocity r is presented instead of Ω. The time indicated on the plots is in terms of full-scale values.

The first calculated results presented are of an attempted spin entry from trimmed flight with both $C_{m_{\dot{\alpha}}}$ and C_{m_q} assumed to be zero. These results are presented in figure 10 along with results from a spin obtained during an airplane flight test. As may be seen from the figure, in comparison with the airplane result, the calculated result indicated a much more oscillatory spinning motion. The movement of ailerons to against the spin after the direction of rotation had been established (moving stick left in an erect spin turning to the pilot's right) was made in both the full-scale flight and in the computer calculation. (See fig. 10.) This movement is typical of the aileron-manipulation technique being used in flight when it is attempted to assure a given direction of spin for many current fighter configurations including the one for this investigation. Analysis of the results of the preliminary calculation indicated that the application of damping in pitch C_{m_q} and $C_{m_{\dot{\alpha}}}$ was desirable to obtain closer agreement with full-scale results.

L 2 1 8

Several arbitrary combinations of C_{m_q} and $C_{m_{\dot{\alpha}}}$ were used for spin entries from trimmed flight. It was found that when these values totaled -0.9 in any combination ranging from $C_{m_{\dot{\alpha}}} = -0.9$ and $C_{m_q} = 0$ to the reverse combination, results fairly similar to the full-scale result were obtained, especially with regard to the important parameter, rotation rate of the spin. The time hisories in figure 11 obtained for $C_{m_{\dot{\alpha}}} = -0.45$ and $C_{m_q} = -0.45$ illustrate these results. Recovery was attempted (fig. 11) at $\alpha = 70^\circ$ and $r = 0.98$ radian/sec ($\Omega = 0.167$ rps) by reversing ailerons and rudder simultaneously. These controls were applied after about $3\frac{1}{3}$ turns of the spin, as were the airplane controls during the flight tests. A recovery was obtained in $1\frac{9}{10}$ turns (fig. 11) which was in qualitative agreement with the full-scale result $\left(1\frac{2}{3}\right)$ given in the section entitled "ANALYSIS, METHODS, AND CALCULATIONS."

For the calculated spin, the angle of attack and rate of rotation at the time of recovery-control application (fig. 11) was still increasing somewhat. Therefore, an additional calculation was made in which the same spin was allowed to continue several additional turns (a total of eight turns from initial entry) before recovery controls were applied. (See fig. 12.) Although the angle of attack and rate of rotation were still increasing very slowly (α was 73.5° and Ω was 1.15 radians/sec or 0.19 rps), it appeared that an approximate equilibrium spin had been achieved. The slight changes still present in the motion (fig. 12) were probably due to the fact that the residual oscillations from spin entry

had not yet given way to complete spin equilibrium and also possibly due to the fact that air density was increasing as altitude was lost. At this time (eight turns after initiating spin entry) a recovery attempt was made, and a $2\frac{1}{2}$-turn recovery resulted (fig. 12). This recovery is also considered to be in good qualitative agreement with the full-scale flight results even though the spin was allowed to progress nearly five turns longer than the airplane had spun. The increase in Ω shown at the end of the calculated spin in figure 12 resulted from a rolling motion which occurred after the recovery from the spin.

The results of a calculation made to simulate a spin using the spin-tunnel entry technique are shown in figure 13. For this calculation, $C_{m_{\dot{\alpha}}} = -0.45$ and $C_{m_q} = -0.45$ were used. As can be seen in the figure, after the launching with rotation, the model initially spun flat and fast and began to steepen and slow its rotation gradually. After about 50 turns, it appeared as though the motion was tending asymptotically toward a spin similar to that obtained from trimmed-flight spin-entry calculations. Because of high inertias, 50 turns may sometimes be required for a spin-tunnel model of a current fighter-type airplane to achieve spin equilibrium following a rapid-rotation launching in the spin tunnel. The near equilibrium angle of attack and rate of rotation indicated after about 50 turns were slightly higher than those for the calculated spin at the end of eight turns after trimmed flight entry. It appeared that these differences could be due to the difference in air density since this calculation was for a constant altitude of 40,000 feet and since the spin obtained from trimmed flight entry was at an altitude of about 25,000 feet at the end of eight turns. In order to check on this apparent effect of air density, a calculation was made in which the eight-turn spin calculated from trimmed flight entry was allowed to continue with the air density abruptly set constant at the value for 40,000 feet. The spin soon changed to become similar to the spin (fig. 13) obtained with the use of the spin-tunnel launching technique. This result is presented in figure 14. As may be seen, the calculated motion was oscillatory due to the abrupt disturbance which had been applied, but the oscillations were being slowly damped when the calculation was terminated to save machine-computing time. The indicated effect of air density on spin characteristics is similar to the effects obtained experimentally on earlier configurations in reference 5.

A recovery was attempted from the spin obtained by simulation of the spin-tunnel model launching technique (fig. 13), and a recovery was obtained in $3\frac{1}{2}$ turns. This recovery was somewhat slower than the $2\frac{1}{2}$-turn recovery obtained by the trimmed flight entry of figure 12. The slow recovery was probably due to a ten-percent increase in the resultant spin rotation rate which was probably caused by the lower air density. Although

for the present configuration the difference in recovery was only one turn, results obtained with a number of free-spinning tunnel models indicate that a difference of ten percent in rate of spin rotation, such as existed prior to the recoveries described, can sometimes mean the difference between rapid recoveries and no recoveries at all. Therefore, it appears that the rate of spin rotation obtained and hence the turns required for recovery may be influenced by the fact that in spin-tunnel testing the variation of air density with altitude is not simulated.

Up to this point it appeared that tunnel technique did not account for the difference in results obtained for the airplane and those obtained for the spin-tunnel model. The results of the calculations appeared, in general, to predict the full-scale results and not those obtained in the tunnel. It was decided to evaluate the effects of variations in the derivative C_{n_r} for two reasons: First, the damping in yaw and the static pitching moment are two very important factors affecting the nature of spins (ref. 1); and, due to difficulties present in obtaining measured rotary derivatives such as C_{n_r} as compared with the conventional static wind-tunnel measurements used to obtain C_m, values of C_{n_r} are subject to possible inaccuracies. Second, varying C_{n_r} is one way in which possible effects of different Reynolds numbers acting during spins might be simulated in calculations. Variation of other rotary derivatives is also of general research interest, but such calculations were not included within the scope of the present paper. The variations of C_{n_r} plotted against angle of attack are shown in figure 15 and are labelled variations 1, 2, and 3. The nature of these curves was decided arbitrarily. As may be seen in figure 15, the C_{n_r} variation 3 is a smooth curve which is considered to be well within the limits of accuracy of the measured C_{n_r} against α curve. The C_{n_r} variation 1 curve provides generally more damping than the original curve while variation 2 provides less damping than the original only for angles of attack above 25°. All three C_{n_r} variations, however, tended toward the original value at 90° angle of attack.

The results of the calculations made with the use of the C_{n_r} variations 1, 2, and 3 are presented in figures 16 to 18. Both types of entry maneuvers were used in these calculations. As may be seen from figure 16(a), when the magnitude of the damping in yaw was reduced by using the C_{n_r} variation 2 curve, a spin was obtained from trimmed flight entry which rotated a little faster (Ω = 0.194 rps) than that obtained for the same type entry when the original C_{n_r} curve was used. The recovery was a little slower (3.35 turns). However, when the spin-tunnel entry technique was simulated (fig. 16(b)), a higher angle of

attack, more rapidly rotating spin, and poor recovery characteristics were indicated. This spin was similar to the one obtained in the spin tunnel (as indicated in the table in the section entitled "ANALYSIS, METHODS, AND CALCULATIONS.")

When the magnitude of the damping in yaw was increased by using the C_{n_r} variation 1 curve (fig. 17), a "no-spin" ensued following an attempted spin entry from trimmed flight (α went below stall, ϕ became negative due to aileron setting, and turns ceased), whereas when a spin-tunnel launching was simulated, a spin was obtained which had a lower angle of attack (64°), a considerably slower rate of rotation (Ω = 0.138 rps), and a much faster recovery (1/4 turn) than those obtained for the original or variation 2 C_{n_r} curves.

L
2
1
8

As indicated in figure 18, the use of C_{n_r} variation 3 curve resulted in a fairly steep, slow-turning spin (α = 48°, Ω = 0.47 radian/sec or 0.075 rps) with a rapid recovery following entry from trimmed level flight and a flat, rapid spin with poor recovery from the simulated spin-tunnel launching.

The use of the C_{n_r} variations indicated that different spin characteristics could result from the two types of spin entry being used herein, and the C_{n_r} variation curves are considered in general within the limits of accuracy present during the wind-tunnel tests to determine the data for C_{n_r} plotted against α. Therefore, the results of the investigation may be interpreted as indicating that two types of spin equilibrium are possible for the airplane in this investigation: a spin obtained from a trimmed level-flight entry and a flatter, faster rotating spin obtained from a motion such as that given a model in spin-tunnel launchings. The characteristic of having more than one type of spin possible is not unique since two or more types of spins have often been indicated in the past as possible for airplanes from the results of free-spinning-model tests. Unfortunately, the flatter, faster rotating spin, which is potentially more dangerous because it usually makes recovery more difficult if not impossible, apparently is occasionally incurred by airplanes during violent maneuvers such as a yawing divergence or other inadvertent turning motions at a high angle of attack even for configurations for which the steeper, slower spin may be considerably more prevalent.

The relative importance of Reynolds number difference as a possible contributing factor to the differences between airplane and model test results for the configuration is not evident. There may have been some effect; however, as noted previously, the difference in spin entry technique alone is apparently sufficient to cause the difference in spin and recovery characteristics obtained.

It is of general interest that use of C_{n_r} variations 1 and 3 caused, respectively, a no-spin and a slowly rotating spin at lower angles of attack from trimmed flight entry compared with the spin obtained with the use of the original C_{n_r} curve. These results indicate that airplanes could possibly be designed which would not spin or which would spin only steeply and slowly (which would enable, in general, rapid recoveries) through use of some aerodynamic feature whose effects need be present only at high angles of attack. This means that it would not be necessary to compromise aerodynamic characteristics needed for high-speed and maneuvering flight in the normal low-angle-of-attack flight regime in order to eliminate undesirable spinning characteristics. This conclusion is in qualitative agreement with the results discussed in reference 1 and with the results of numerous free-spinning-tunnel model tests. These experimental data have indicated important favorable effects which can be obtained in spins by proper attention to fuselage nose cross-sectional shape or by including a retractable strake or some other such device to control the nature of the air flow over the long fuselage forebodies of modern fighter-type airplanes. Controlling this air flow can force the overall yawing moment contributed by the nose to be a spin-damping moment rather than a spin-propelling moment.

The results as a whole indicate that differences between model and airplane spin testing technique may lead to significant differences between the spin and recovery characteristics. Contributing to these possible differences in spins and recoveries are the different aerodynamic and inertia moments acting during the two types of spin-entry maneuvers, the effects of air density, the effects of variation of air density with altitude, and the effects of Reynolds number on the overall damping or propelling moment in spins. Each configuration studied must therefore be evaluated on its own merits in order to determine predicted spin characteristics as appropriately as possible.

CONCLUDING REMARKS

A high-speed digital computer study has been made to investigate the effects of differences in full-scale-airplane and spin-tunnel-model testing techniques on spins and recoveries obtained for a configuration representative of a current 60° delta-wing fighter-type airplane. Calculations were made to simulate airplane spin entry starting from trimmed level flight and to simulate an airplane spin with the use of the spin-tunnel entry technique. Six-degree-of-freedom equations of motion and data for nonlinear aerodynamic stability derivatives were used.

Results obtained for the design investigated indicate that the method by which a spin is entered may in some instances lead to significant differences in spins and recoveries. The investigation revealed

that different spins may be obtainable from an entry from trimmed level flight and from an entry with applied rotation similar to the method used in testing of a spin-tunnel model. Any difference in results, however, may be dependent upon the directional characteristics of the airplane at spinning attitudes and this could, in turn, be influenced by Reynolds number. Factors contributing to possible differences in spins and recoveries are the different aerodynamic and inertia moments acting during the two types of spin-entry maneuvers, the effects of air density, and the effects of variation of air density with altitude.

The results of the investigation emphasize that, as indicated by spin research of the past few years at Langley Research Center, proper evaluation of full-scale spin and recovery characteristics of modern designs from spin-tunnel tests requires cognizance of both tunnel technique and Reynolds number. The results also indicate that analytical approaches, such as that of the present paper, can serve to augment experimental research work and may aid in obtaining answers to some of the problems associated with spins of modern airplanes.

Langley Research Center,
National Aeronautics and Space Administration,
Langley Field, Va., May 4, 1959.

APPENDIX

EQUATIONS OF MOTION AND ASSOCIATED FORMULAS

The equations of motion used in calculating the spinning motions were:

$$\dot{p} = \frac{I_Y - I_Z}{I_X} qr + \frac{I_{XZ}}{I_X} \dot{r} + \frac{I_{XZ}pq}{I_X} + \frac{\rho V_R^2 Sb}{2I_X} C_{l_\beta}\beta + \frac{\rho V_R Sb^2}{4I_X} C_{l_p}p + \frac{\rho V_R Sb^2}{4I_X} C_{l_r}r + \frac{\rho V_R^2 Sb}{2I_X} \Delta C_{l,r} + \frac{\rho V_R^2 Sb}{2I_X} \Delta C_{l,a}$$

$$\dot{q} = \frac{I_Z - I_X}{I_Y} pr + \frac{I_{XZ}}{I_Y} r^2 - \frac{I_{XZ}}{I_Y} p^2 + \frac{\rho V_R^2 S\bar{c}}{2I_Y} C_m + \frac{\rho V_R S\bar{c}^2}{4I_Y} C_{m_q}q + \frac{\rho V_R S\bar{c}^2}{4I_Y} C_{m_{\dot{\alpha}}}\dot{\alpha} + \frac{\rho V_R^2 S\bar{c}}{2I_Y} \Delta C_{m,e}$$

$$\dot{r} = \frac{I_X - I_Y}{I_Z} pq + \frac{I_{XZ}}{I_Z} \dot{p} - \frac{I_{XZ}}{I_Z} qr + \frac{\rho V_R^2 Sb}{2I_Z} C_{n_\beta}\beta + \frac{\rho V_R Sb^2}{4I_Z} C_{n_r}r + \frac{\rho V_R Sb^2}{4I_Z} C_{n_p}p + \frac{\rho V_R^2 Sb}{2I_Z} \Delta C_{n,r} + \frac{\rho V_R^2 Sb}{2I_Z} \Delta C_{n,a}$$

$$\dot{u} = -g \sin \theta_e + vr - wq + \frac{\rho V_R^2 S}{2m} C_X + \frac{\rho V_R^2 S}{2m} \Delta C_{X,e}$$

L
2
1
8

$$\dot{v} = g \cos \theta_e \sin \phi_e + wp - ur + \frac{\rho V_R^2 S}{2m} C_{Y_\beta} \beta + \frac{\rho V_R^2 S}{2m} \Delta C_{Y,r} + \frac{\rho V_R^2 S}{2m} \Delta C_{Y,a}$$

$$\dot{w} = g \cos \theta_e \cos \phi_e + uq - vp + \frac{\rho V_R^2 S}{2m} C_Z + \frac{\rho V_R^2 S}{2m} \Delta C_{Z,e}$$

In addition, the following formulas were used:

$$\alpha = \tan^{-1} \frac{w}{u}$$

$$\beta = \sin^{-1} \frac{v}{V_R}$$

$$V_R = \sqrt{u^2 + v^2 + w^2}$$

$$\Omega = \sqrt{p^2 + q^2 + r^2}$$

$$V = -u \sin \theta_e + v \cos \theta_e \sin \phi_e + w \cos \theta_e \cos \phi_e$$

$$h_2 = h_1 - \Delta t \, V$$

$$\dot{\theta}_e = q \cos \phi_e - r \sin \phi_e$$

$$\dot{\phi}_e = p + r \tan \theta_e \cos \phi_e + q \tan \theta_e \sin \phi_e$$

$$\dot{\psi}_e = \frac{\dot{\phi}_e - p}{\sin \theta_e}$$

$$\text{Turns in spin} = \frac{\int \dot{\psi}_e \, dt}{2\pi}$$

$$\phi_e = \sin^{-1} \frac{\sin \phi}{\cos \theta_e}$$

REFERENCES

1. Neihouse, Anshal I., Klinar, Walter J., and Scher, Stanley H.: Status of Spin Research for Recent Airplane Designs. NACA RM L57F12, 1957.

2. Hewes, Donald E.: Low-Speed Measurement of Static Stability and Damping Derivatives of A 60° Delta-Wing Model for Angles of Attack of 0° to 90°. NACA RM L54G22a, 1954.

3. Polhamus, Edward C.: Effect of Flow Incidence and Reynolds Number On Low-Speed Aerodynamic Characteristics of Several Noncircular Cylinders With Applications to Directional Stability and Spinning. NACA TN 4176, 1958.

4. Polhamus, Edward C., Geller, Edward W., and Grunwald, Kalman J.: Pressure and Force Characteristics of Noncircular Cylinders as Affected by Reynolds Number With a Method Included for Determining the Potential Flow About Arbitrary Shapes. NASA TR R-46, 1959.

5. Seidman, Oscar, and Neihouse, A. I.: Free-Spinning Wind-Tunnel Tests of a Low-Wing Monoplane With Systematic Changes in Wings and Tails. V. Effect of Airplane Relative Density. NACA Rep. 691, 1940.

TABLE I.- MASS AND DIMENSIONAL CHARACTERISTICS OF AIRPLANE

$\bar{c}$, ft	23.755
b, ft	38.12
S, sq ft	695.05
W, lb	24,811
Center-of-gravity location, percent $\bar{c}$	30.0
I_X, slug-ft^2	13,600
I_Y, slug-ft^2	128,000
I_Z, slug-ft^2	138,000
I_{XZ}, slug-ft^2	4,340
$\frac{I_X - I_Y}{mb^2}$	$-1,021 \times 10^{-4}$
$\frac{I_Y - I_Z}{mb^2}$	-89×10^{-4}
$\frac{I_Z - I_X}{mb^2}$	$1,110 \times 10^{-4}$
Maximum control deflections:	
δ_e, deg	-25
δ_r, deg	±25
δ_a, deg	±7

TABLE II.- VALUES OF VARIABLES AT ZERO TIME IN CALCULATIONS

	Simulated entry from trimmed flight	Simulated spin-tunnel model launching
α, deg	18	87
β, deg	0	0
u, ft/sec	371	16.2
v, ft/sec	0	0
w, ft/sec	120.6	309.6
p, radians/sec	0	0.1255
q, radians/sec	0	0
r, radians/sec	0	2.395
θ_e, deg	18	-3.0
ϕ, deg	0	0
δ_e, deg	$-6\frac{1}{2}$	-25
δ_r, deg	0	25
δ_a, deg	0	± 7
ρ (altitude of 40,000 ft), slug/cu ft	0.000582	0.000582

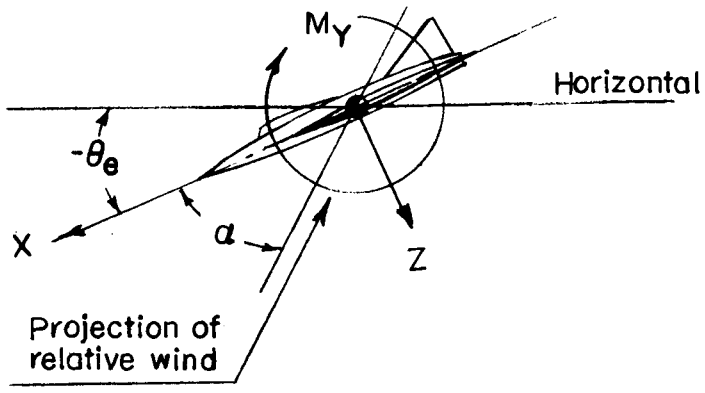

(a) ϕ_e and $\psi_e = 0$.

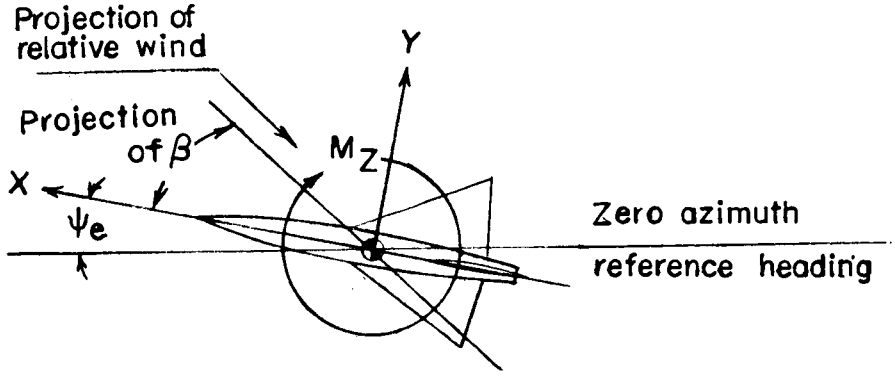

(b) θ_e and $\phi_e = 0$.

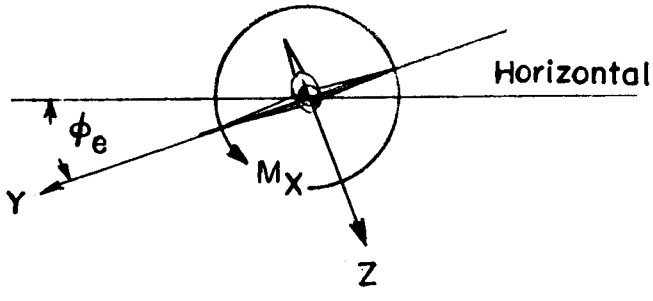

(c) θ_e and $\psi_e = 0$, and in this case $\phi = \phi_e$.

Figure 1.- Body system of axes and related angles.

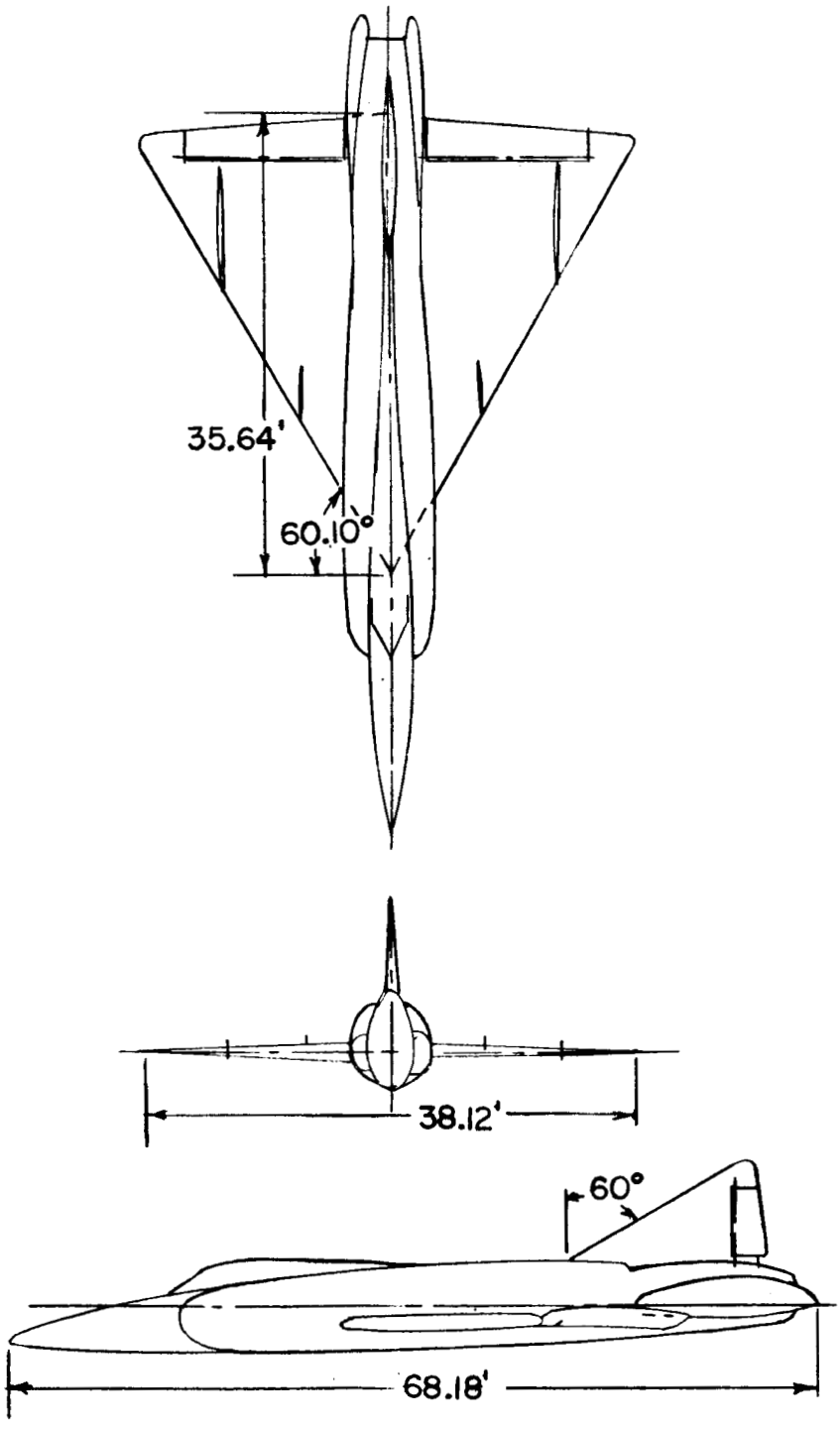

Figure 2.- Three-view sketch of configuration.

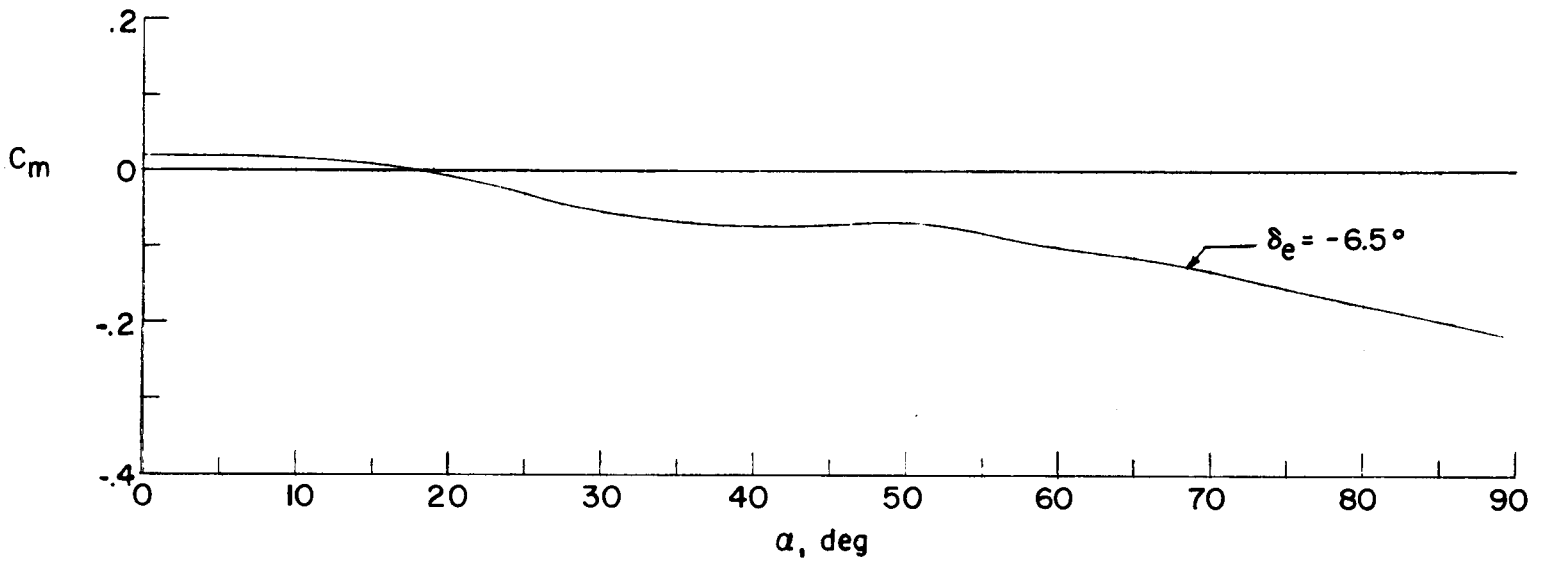

(a) C_m for 30 percent $\bar{c}$.

Figure 3.- Variations of pitching-moment, normal-force, and longitudinal-force coefficients with angle of attack.

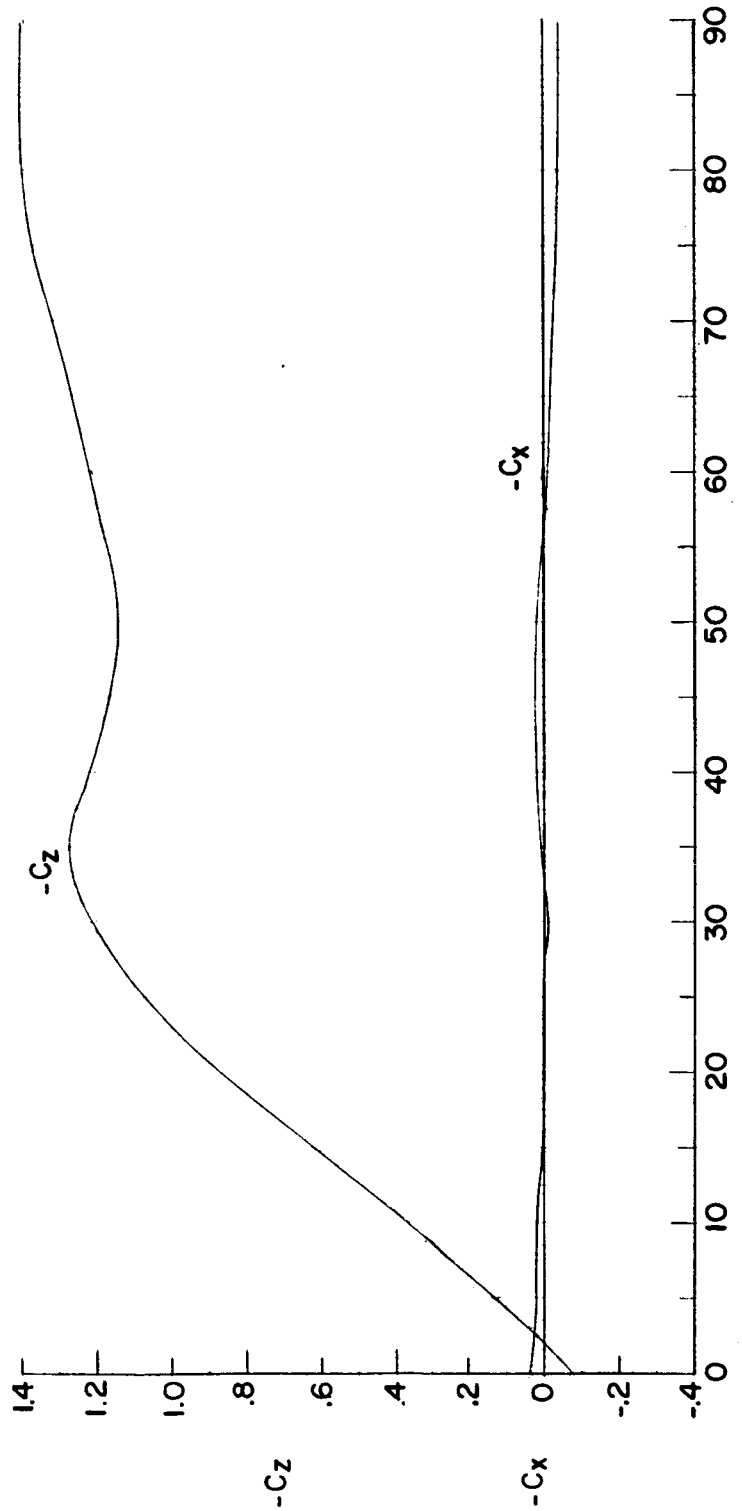

(b) C_Z and C_X.

Figure 3.- Concluded.

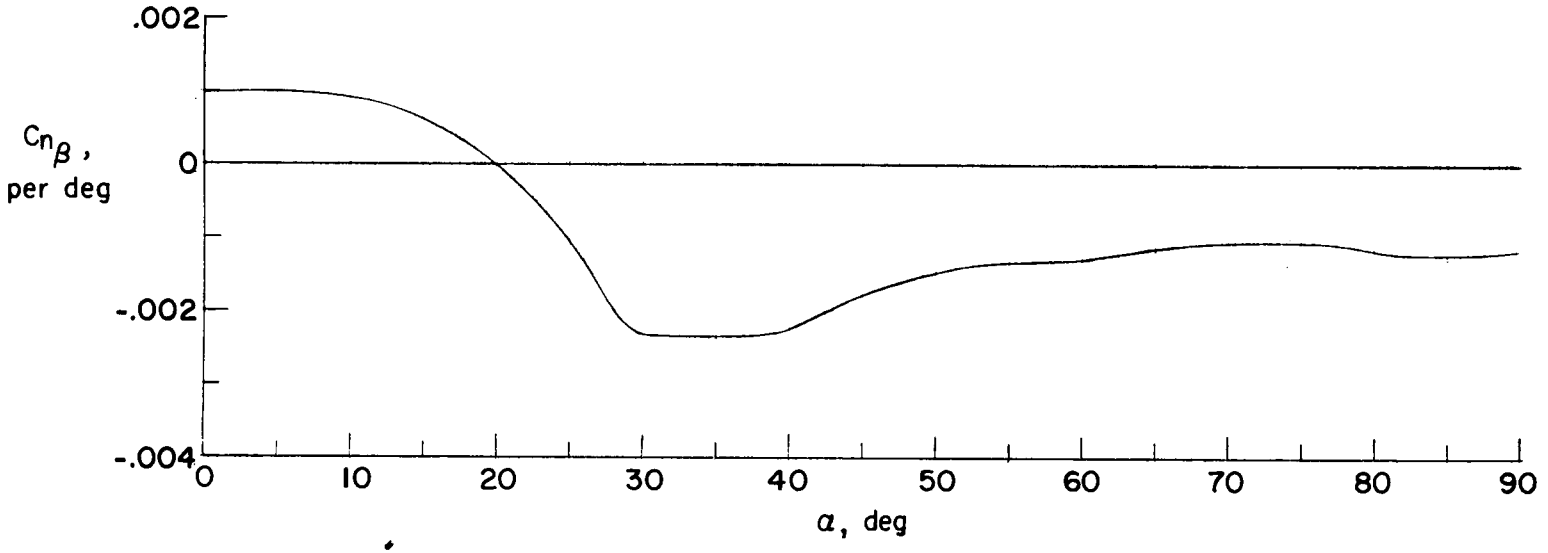

(a) C_{n_β}.

Figure 4.- Variation of the sideslip derivatives with angle of attack.

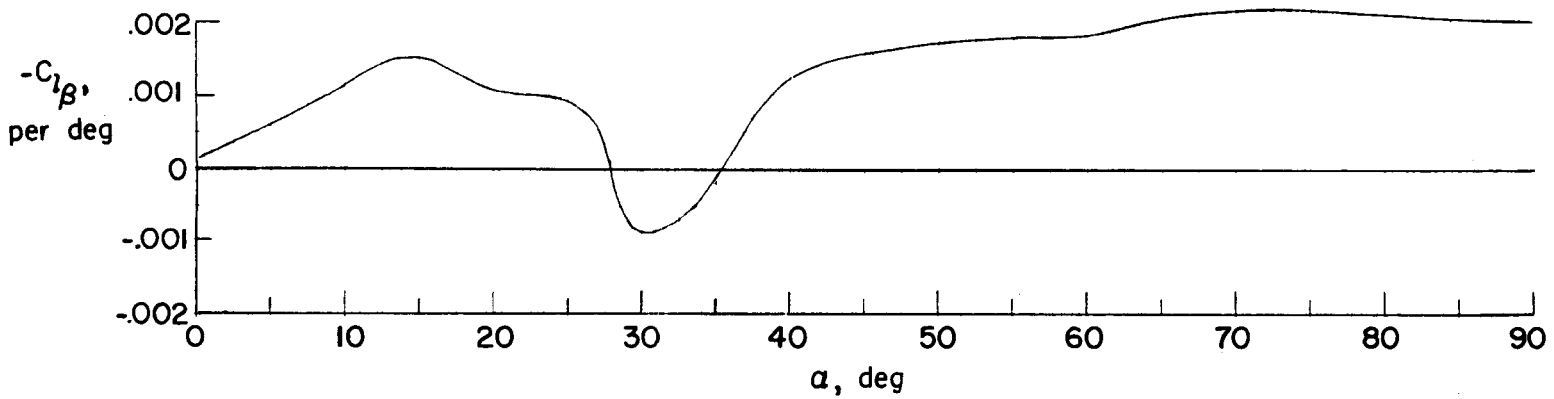

(b) C_{l_β}.

Figure 4.- Continued.

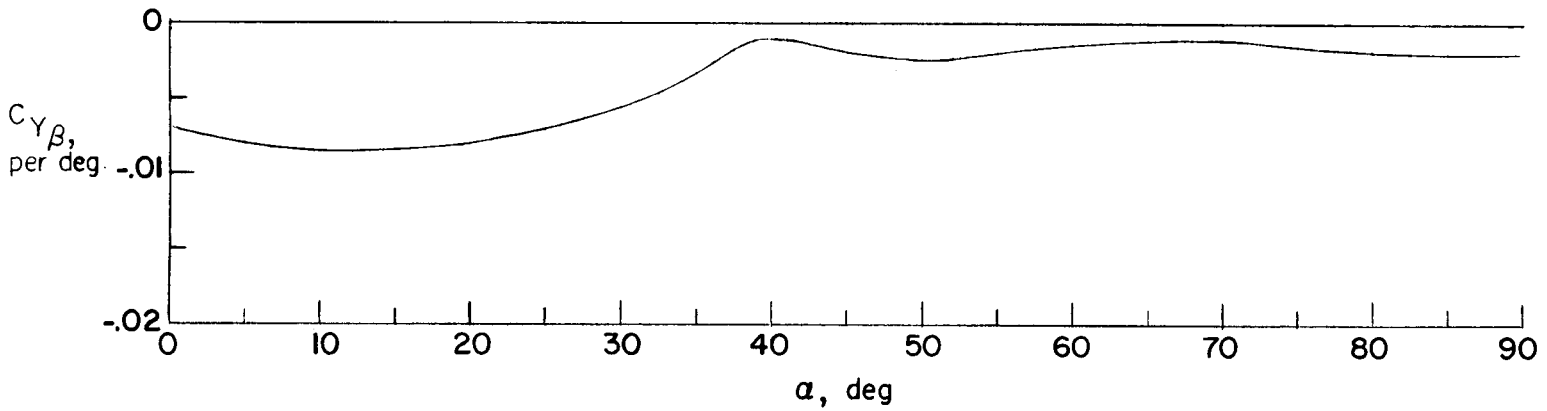

(c) C_{Y_β}.

Figure 4.- Concluded.

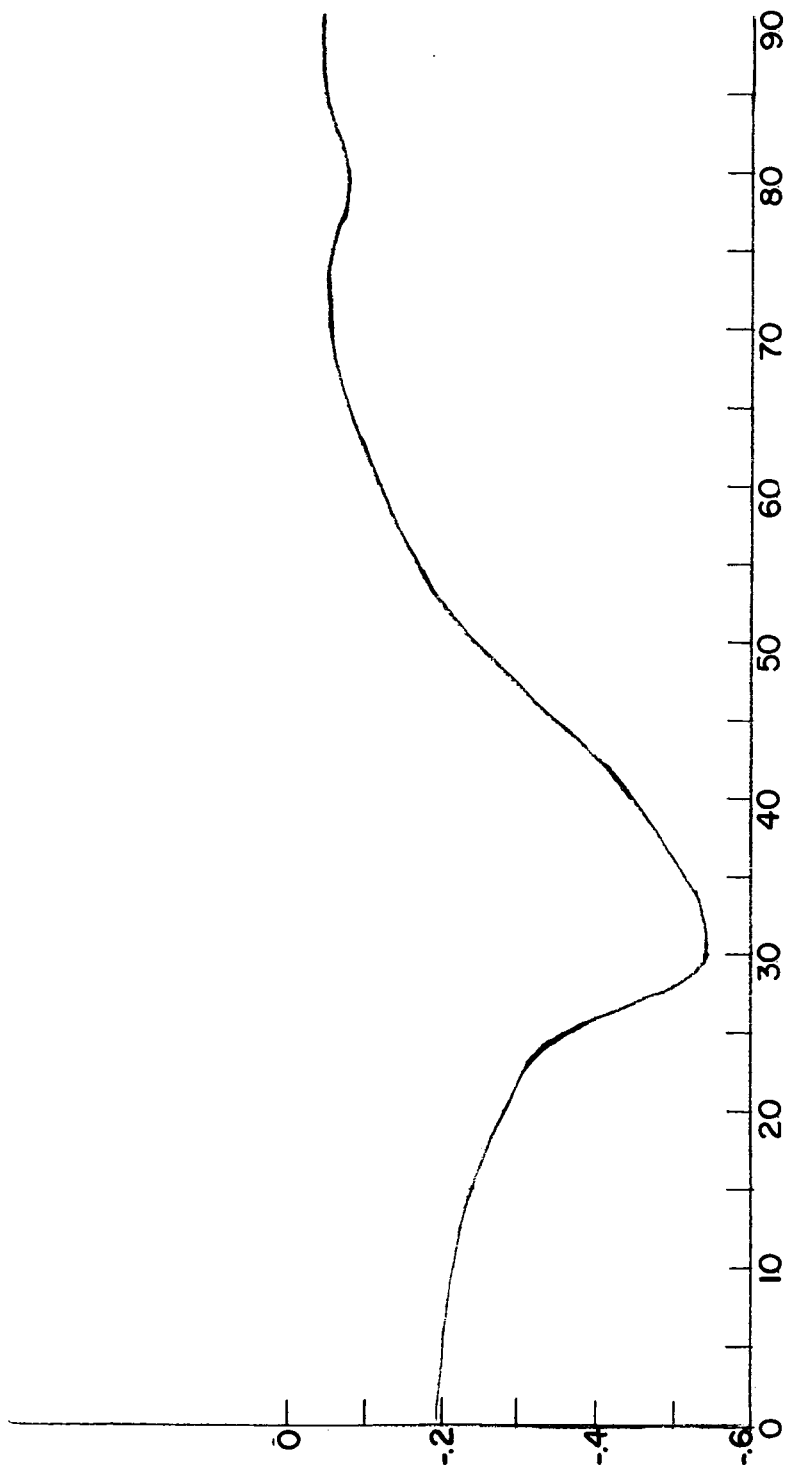

(a) C_{n_r}.

Figure 5.- Variations of the damping in yaw and damping in roll derivatives with angle of attack.

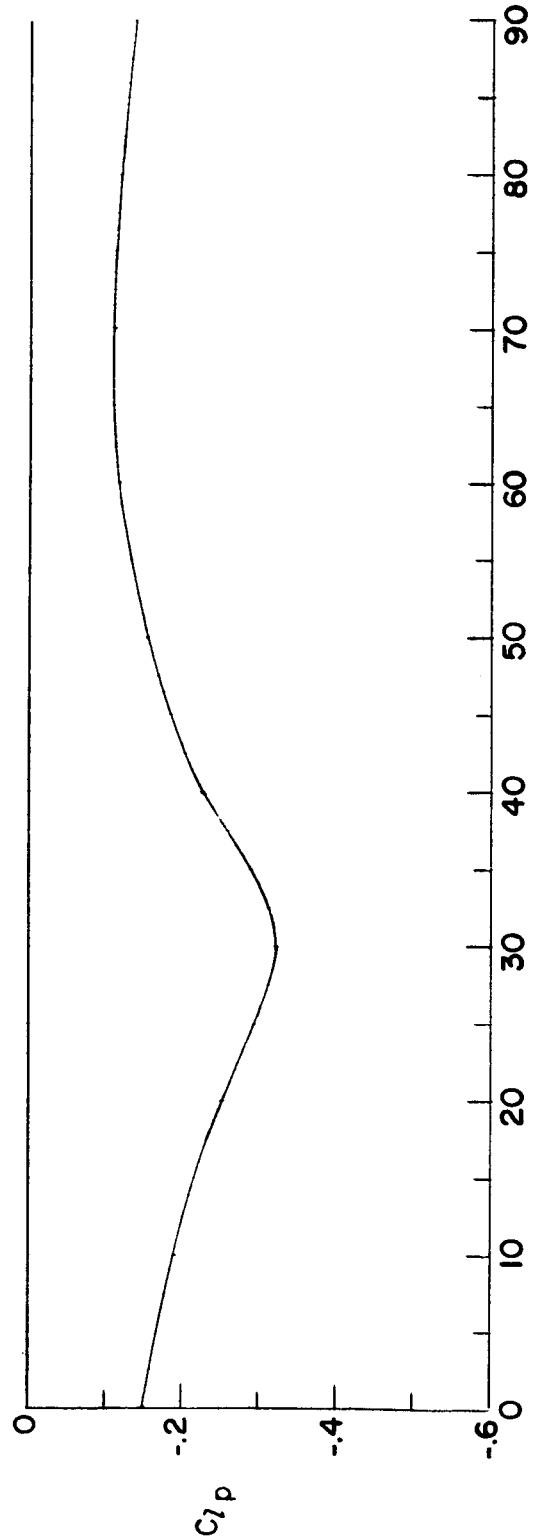

(b) C_{l_p}.

Figure 5.- Concluded.

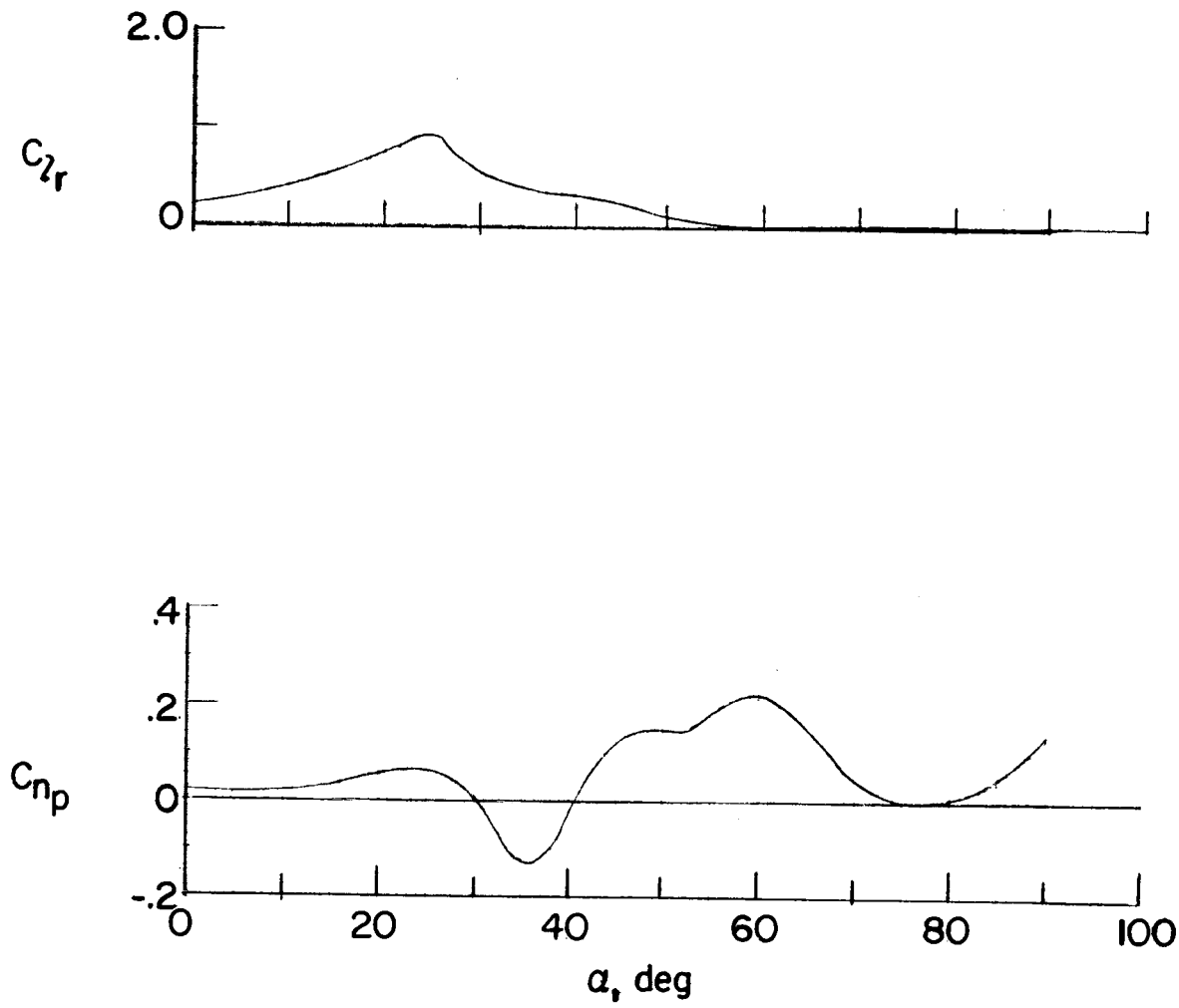

Figure 6.- Variations of the rolling moment due to yawing and the yawing moment due to rolling with angle of attack.

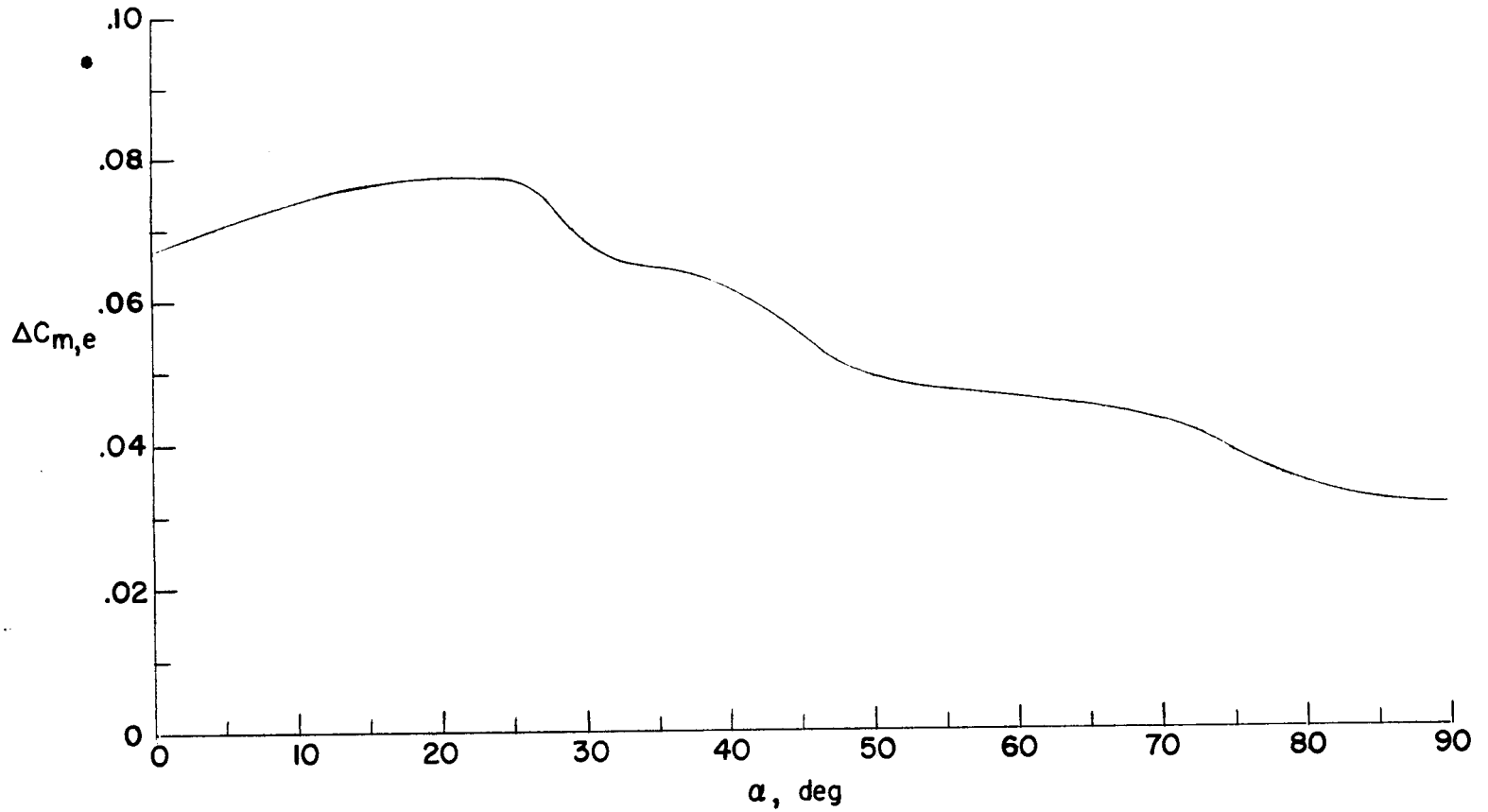

(a) $\Delta C_{m,e}$.

Figure 7.- Variation in increments of pitching-moment and normal- and longitudinal-force coefficients due to deflecting elevators from $-6\frac{1}{2}^{\circ}$ to -25°.

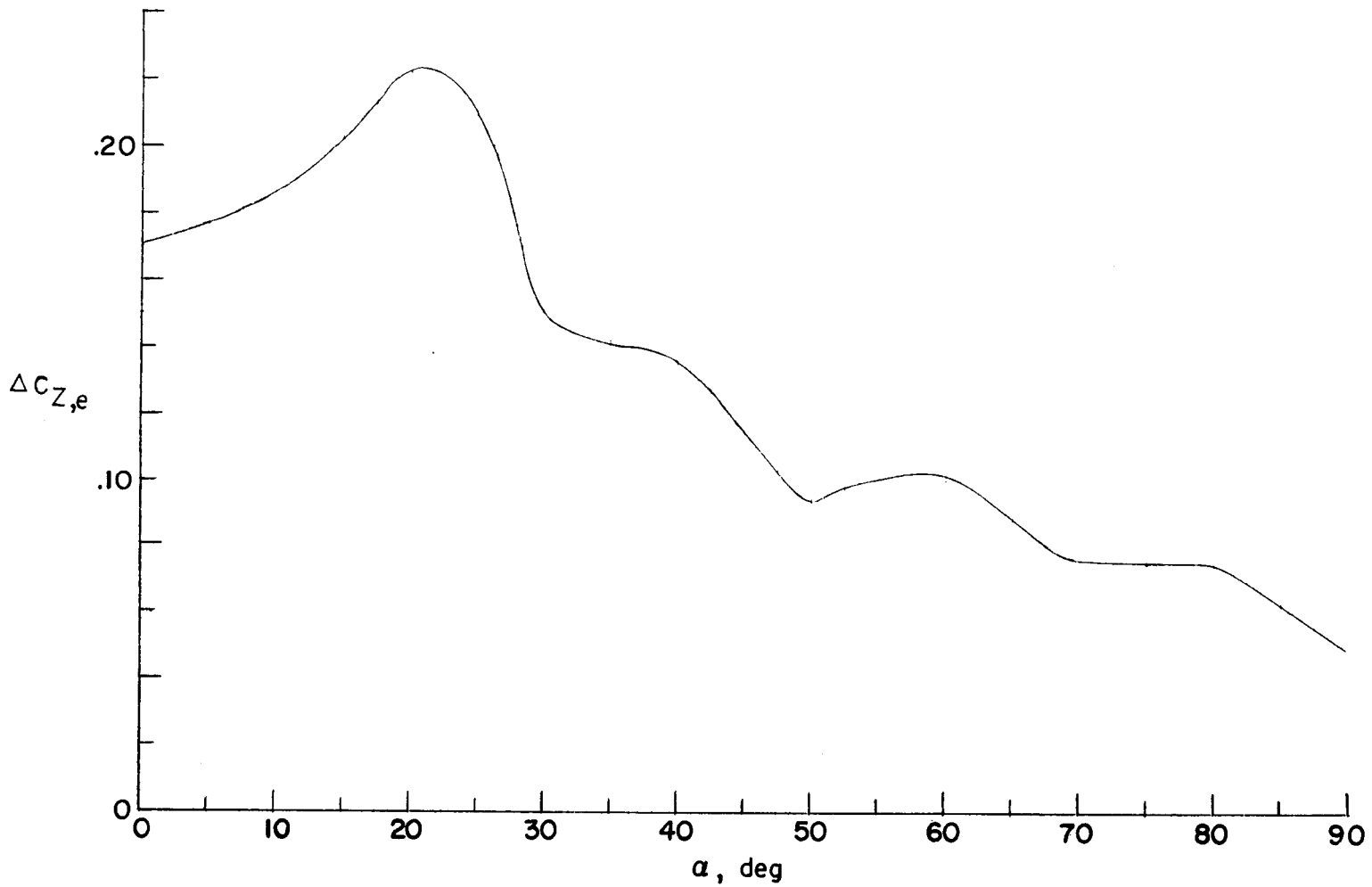

(b) $\Delta C_{Z,e}$.

Figure 7.- Continued.

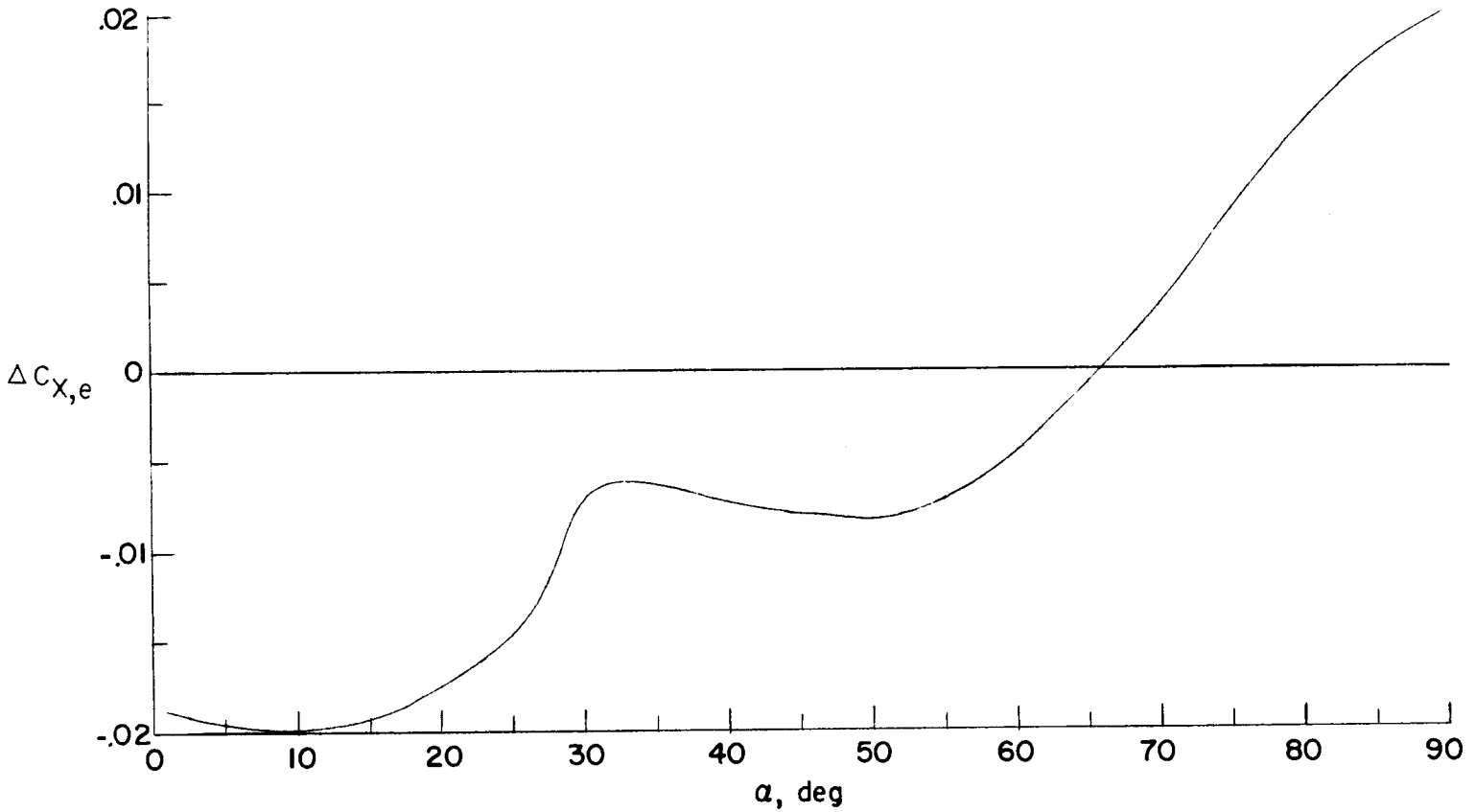

(c) $\Delta C_{X,e}$.

Figure 7.- Concluded.

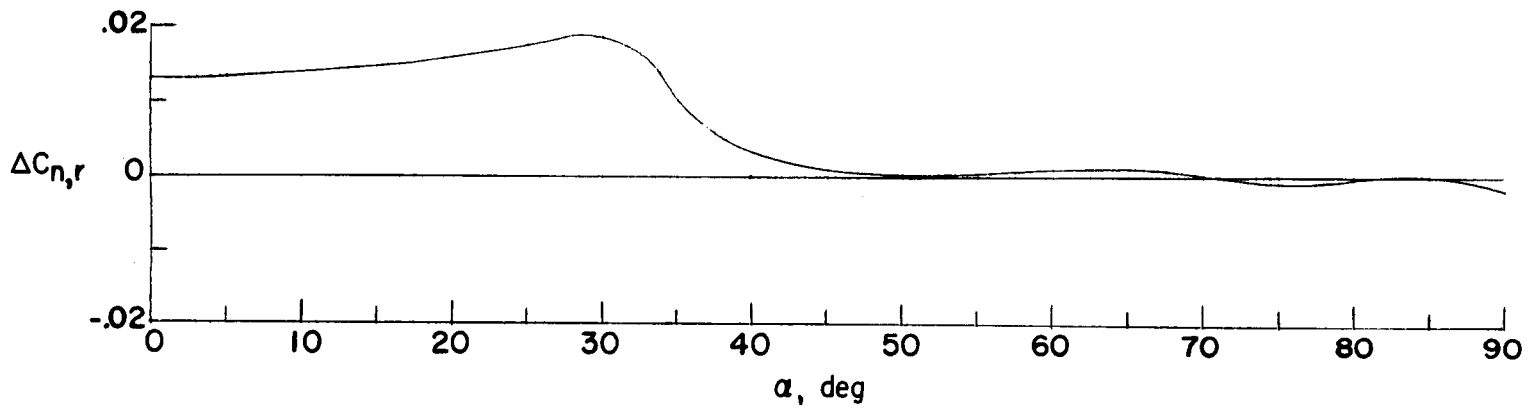

(a) $\Delta C_{n,r}$.

Figure 8.- Variation in increments in the lateral force and moment coefficients with angle of attack due to deflecting rudder. Rudder deflection, 25° right.

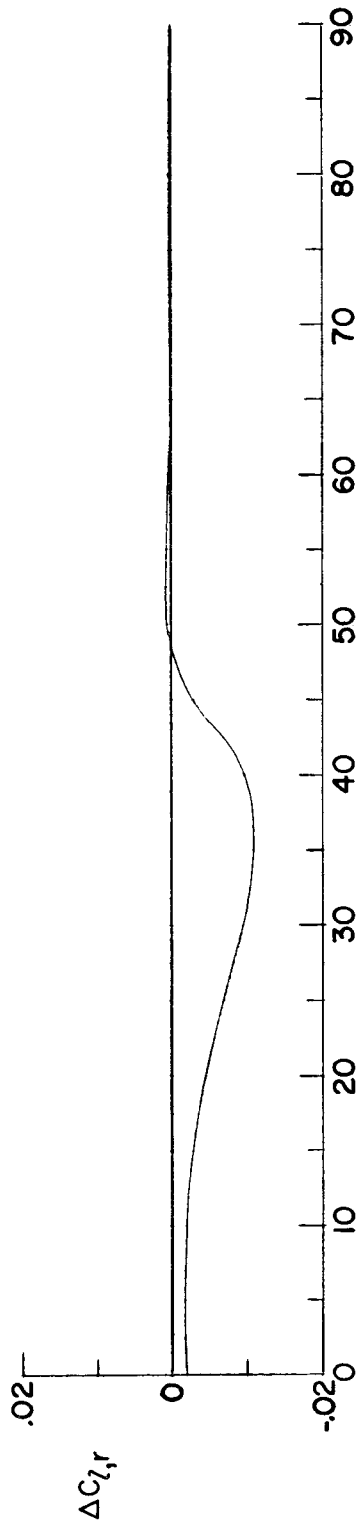

(b) $\Delta C_{l,r}$.

Figure 8.- Continued.

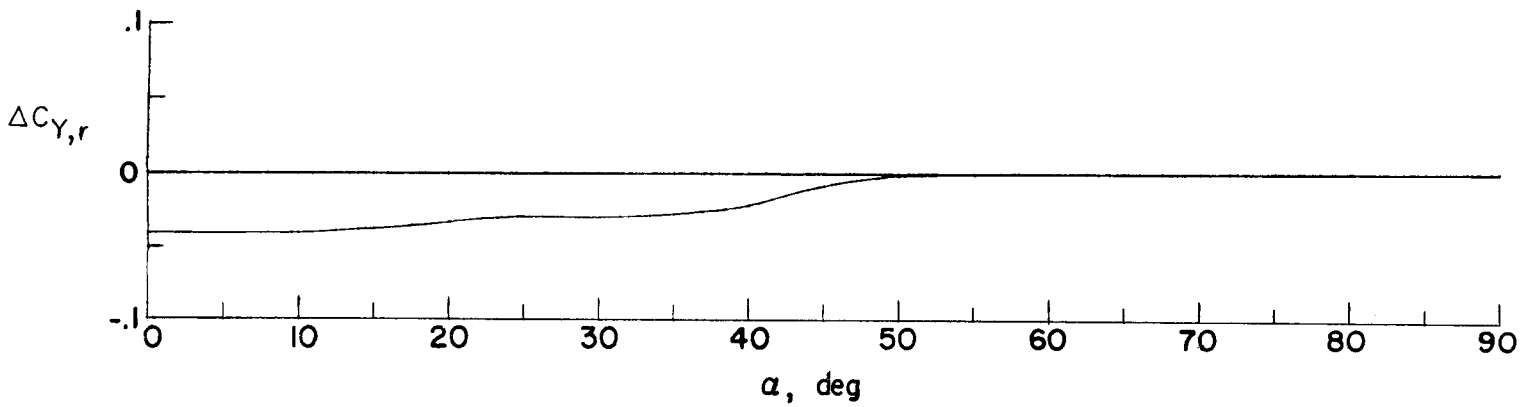

(c) $\Delta C_{Y,r}$.

Figure 8.- Concluded.

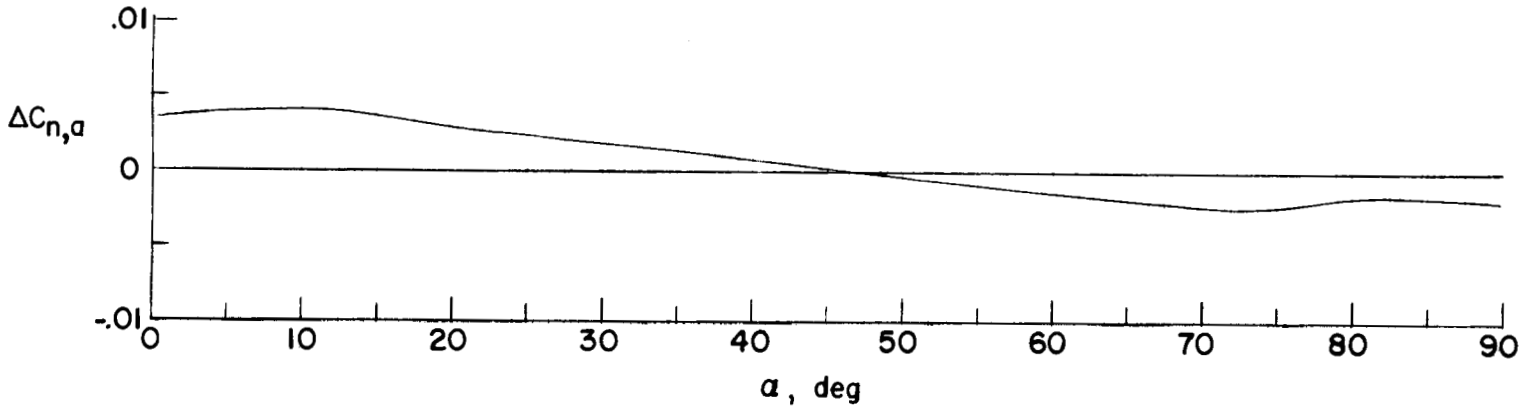

(a) $\Delta C_{n,a}$.

Figure 9.- Increments in the lateral force and moment coefficients due to deflecting ailerons. Aileron deflection $\pm 7^{\circ}$ with right spin.

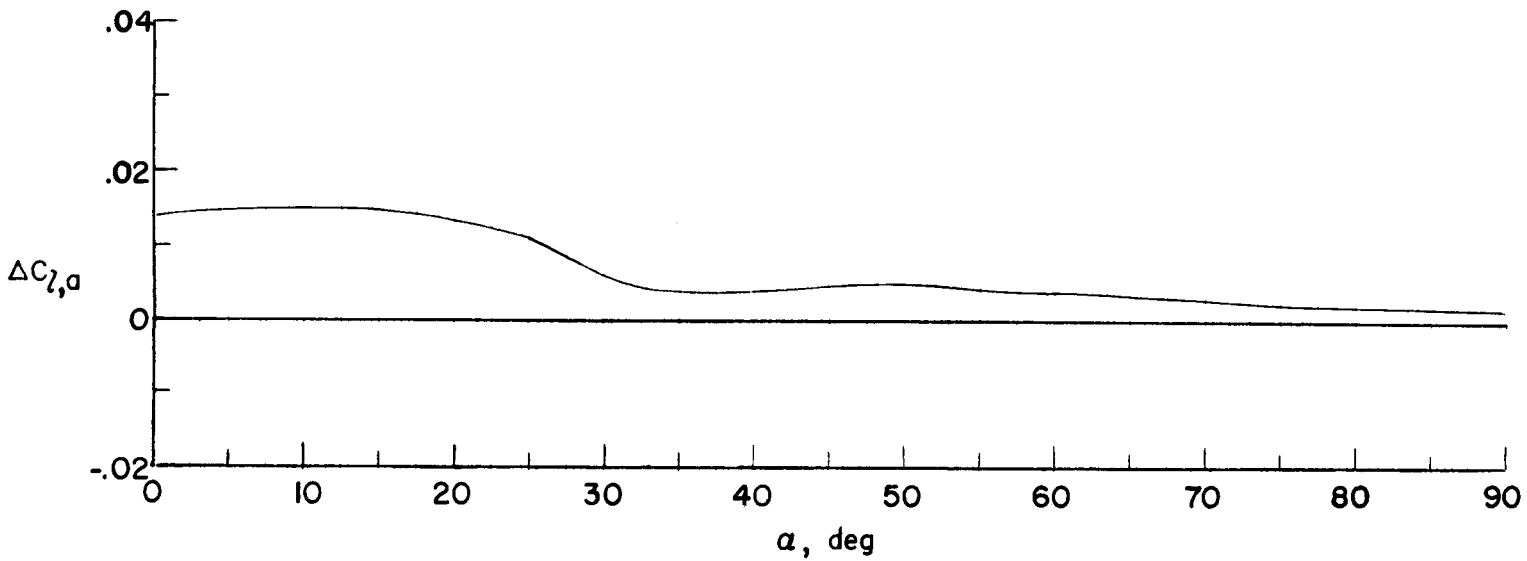

(b) $\Delta C_{l,a}$.

Figure 9.- Continued.

(c) $\Delta C_{Y,a}$.

Figure 9.- Concluded.

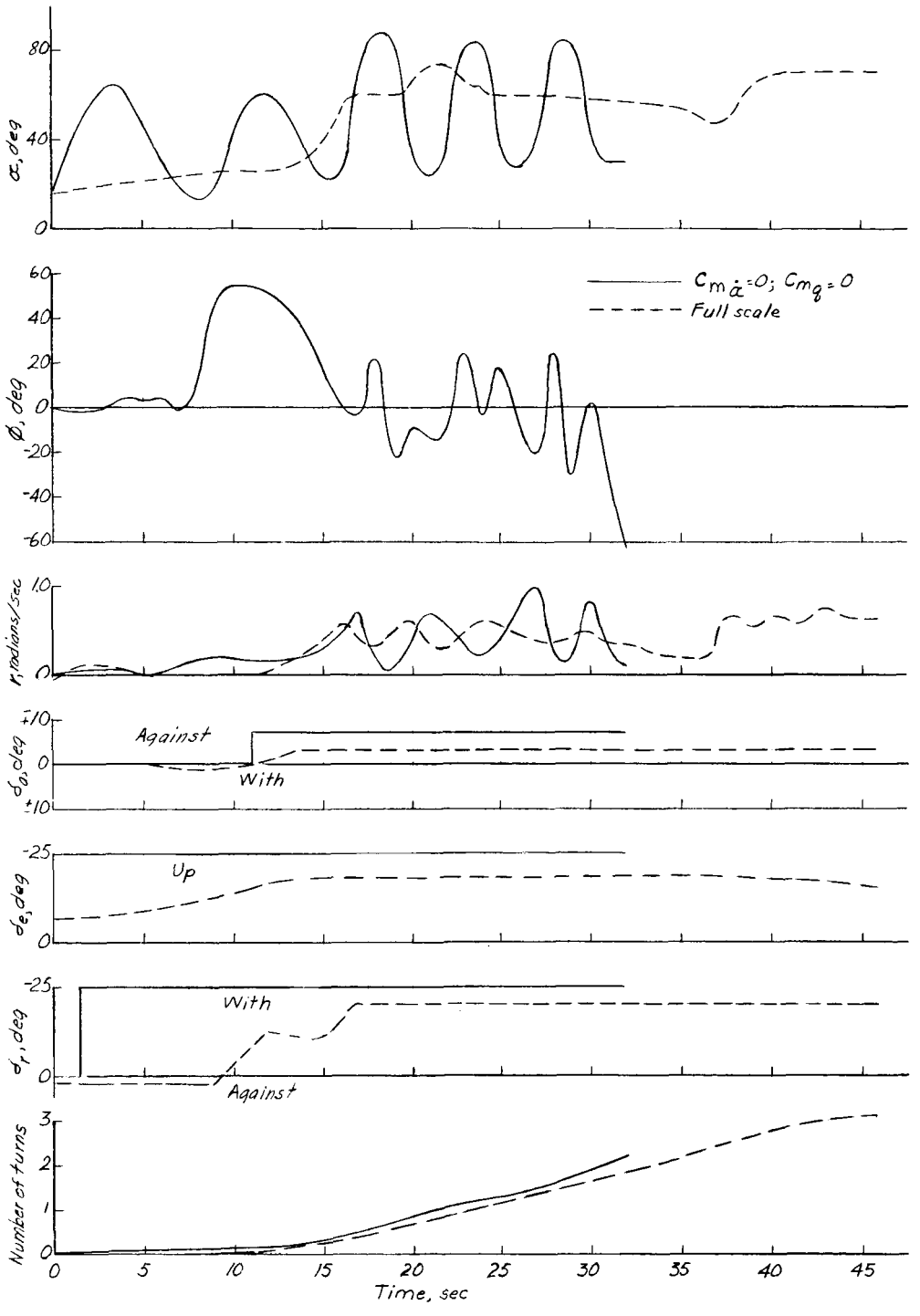

Figure 10.- Comparison of full-scale flight test with initial calculated spin entry.

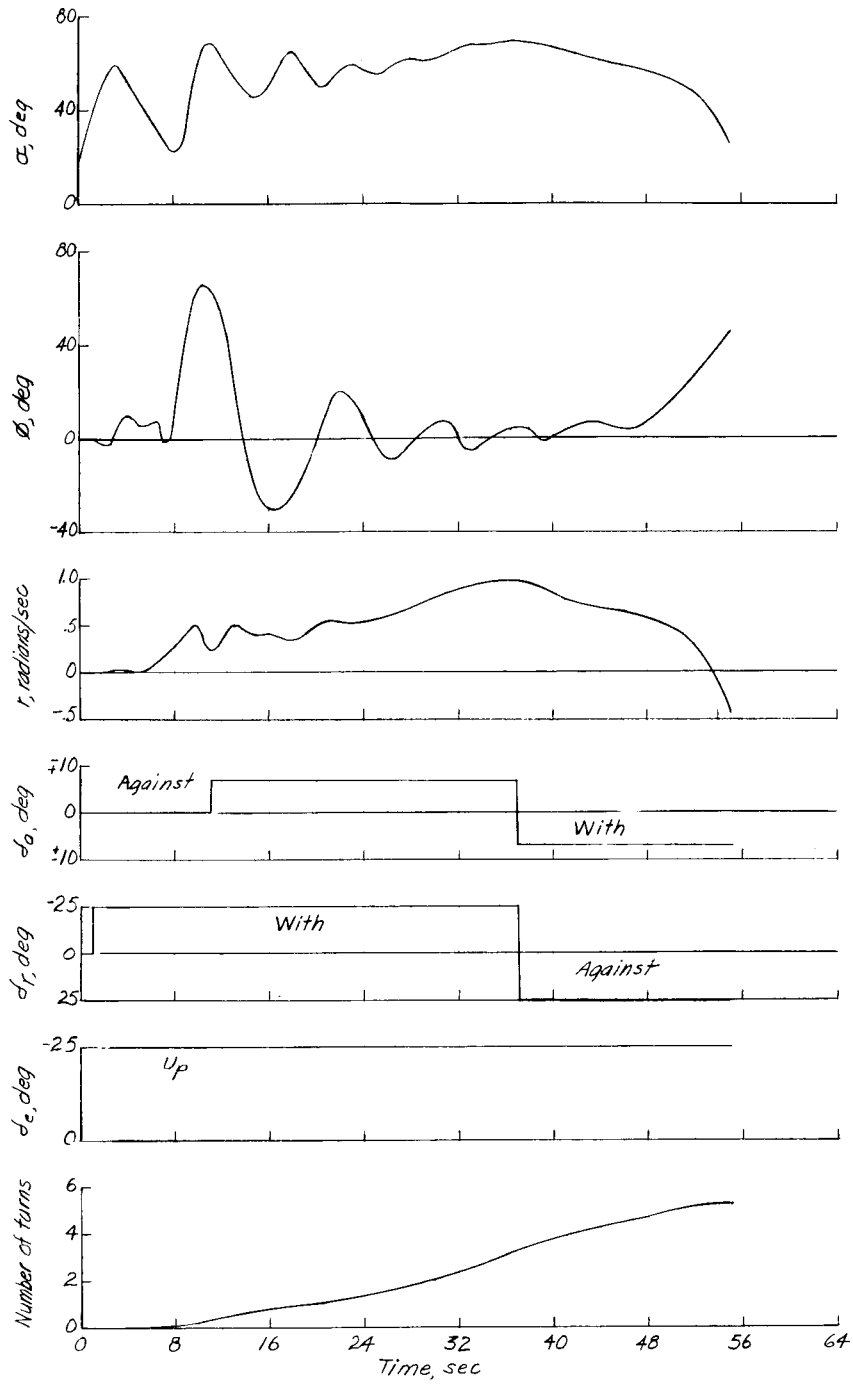

Figure 11.- Calculated $3\frac{1}{3}$-turn spin, including entry from trimmed flight, and recovery. $C_{m_{\dot{\alpha}}} = -0.45$; $C_{m_q} = -0.45$.

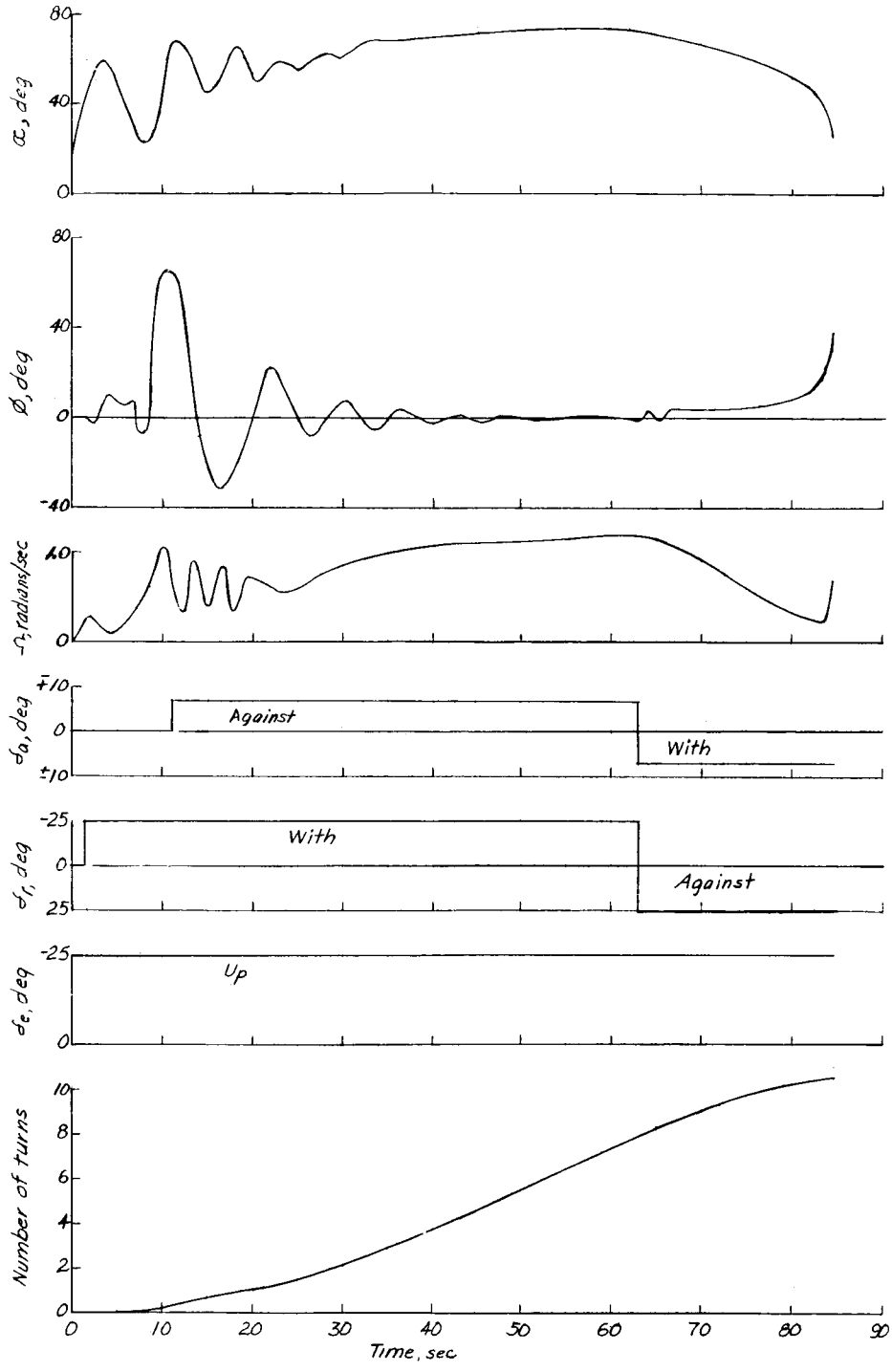

Figure 12.- Calculated 8-turn spin, including entry from trimmed flight, and recovery. $C_{m_{\dot{\alpha}}} = -0.45$; $C_{m_q} = -0.45$.

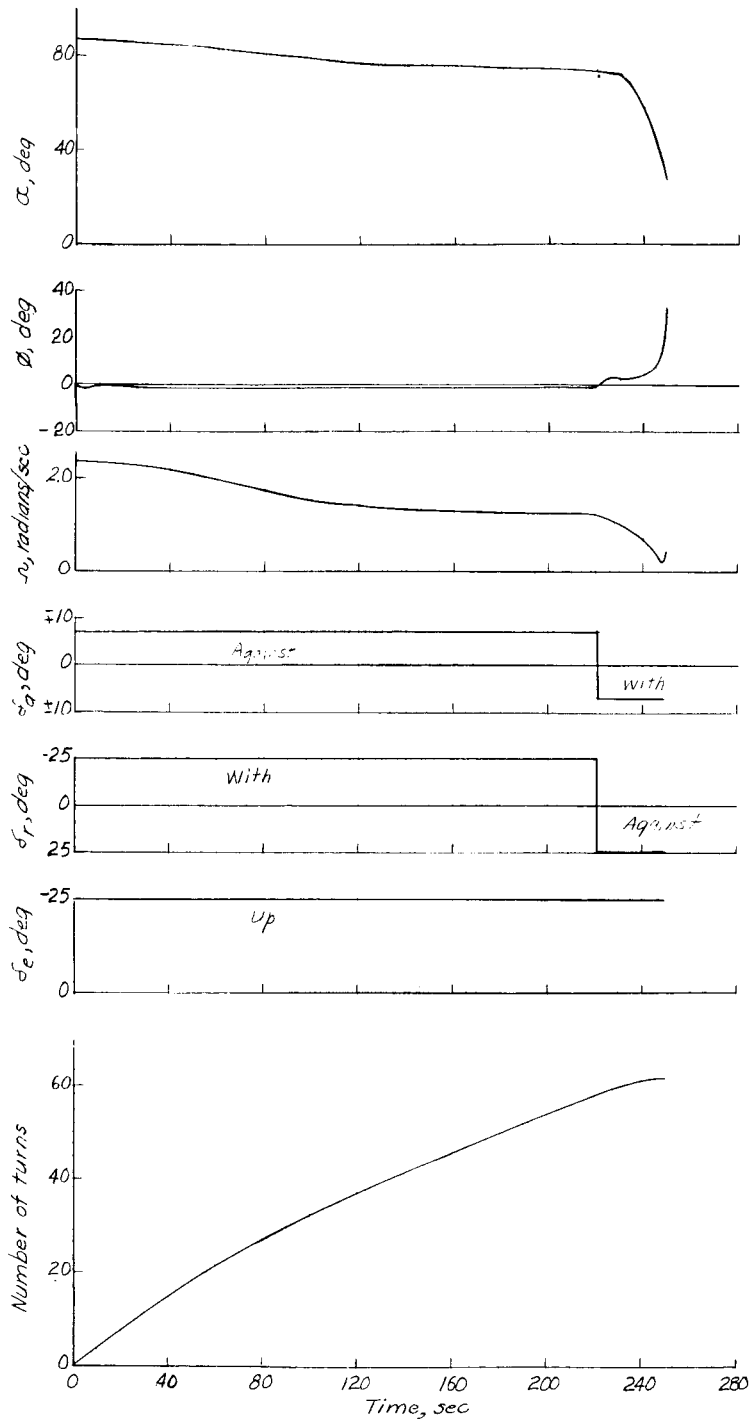

Figure 13.- Calculated spin and recovery using simulated model launching technique. $C_{m_{\dot{\alpha}}} = -0.45$; $C_{m_q} = -0.45$.

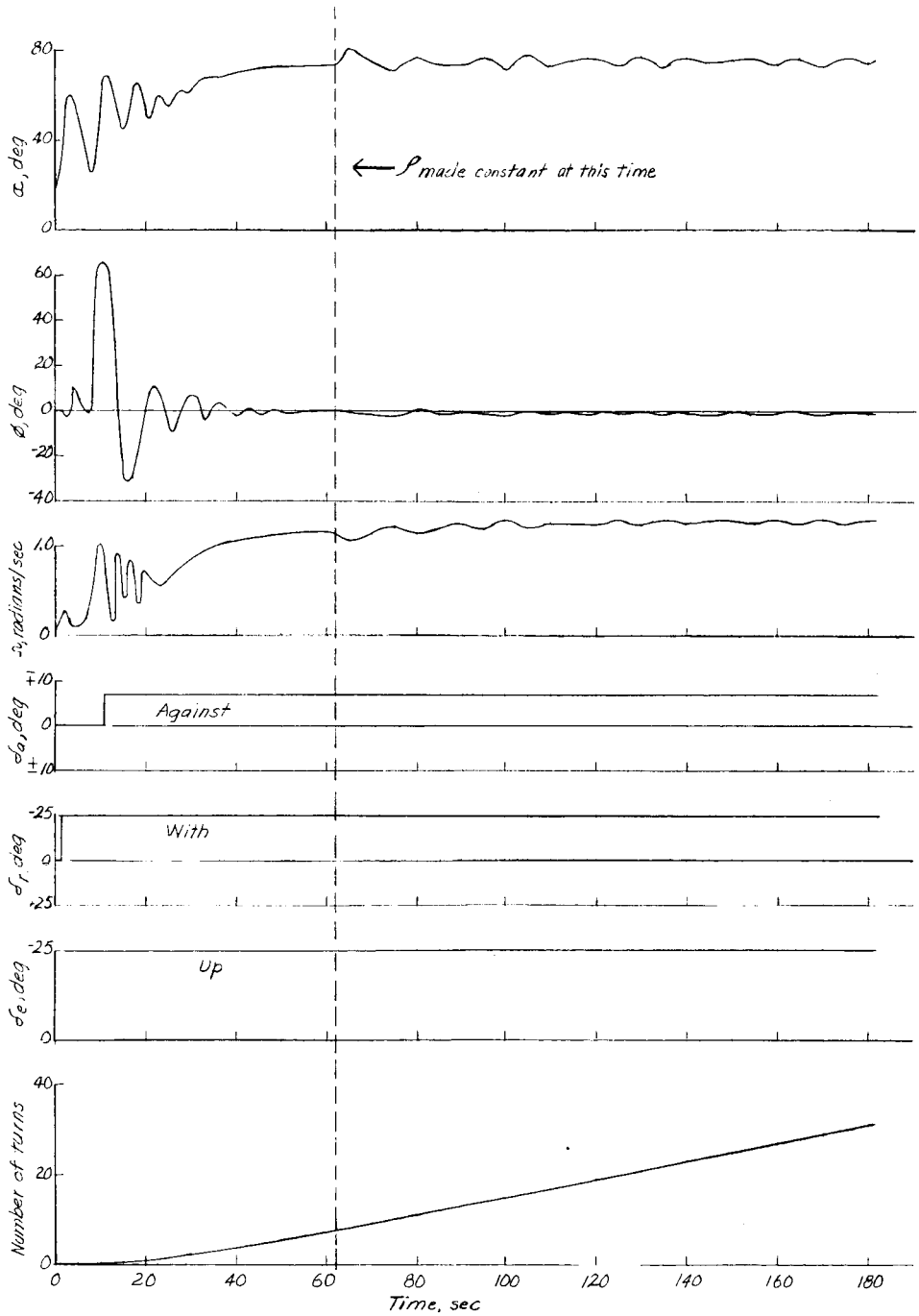

Figure 14.- Calculated spin entered from trimmed flight and continued with altitude of 40,000 feet (ρ = 0.000582) after 8 turns. $C_{m_{\dot{\alpha}}}$ = -0.45; C_{m_q} = -0.45.

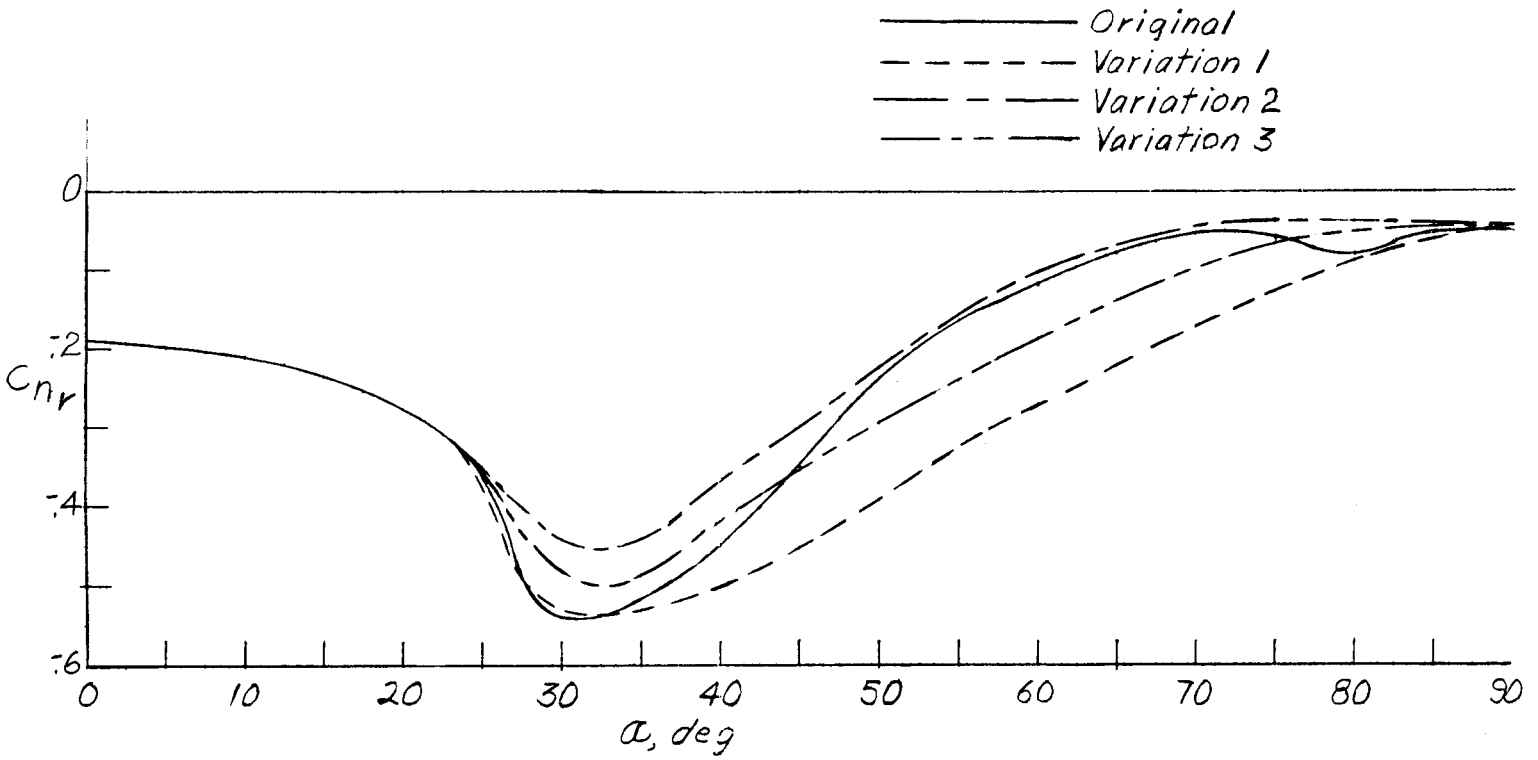

Figure 15.- Variations of C_{n_r} with angle of attack.

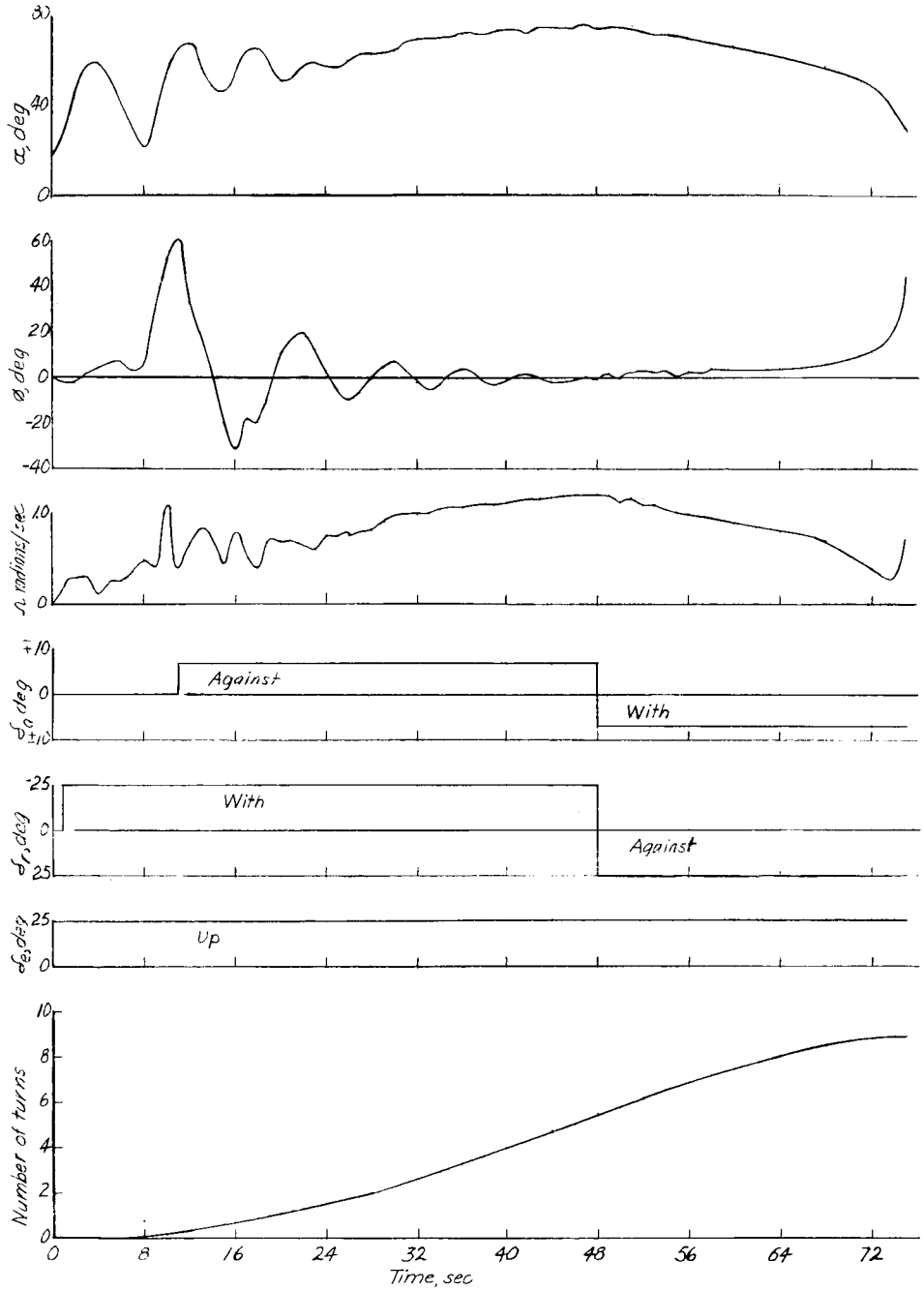

(a) Spin entry from trimmed flight.

Figure 16.- Calculated spins and recoveries with use of C_{n_r} variation 2.

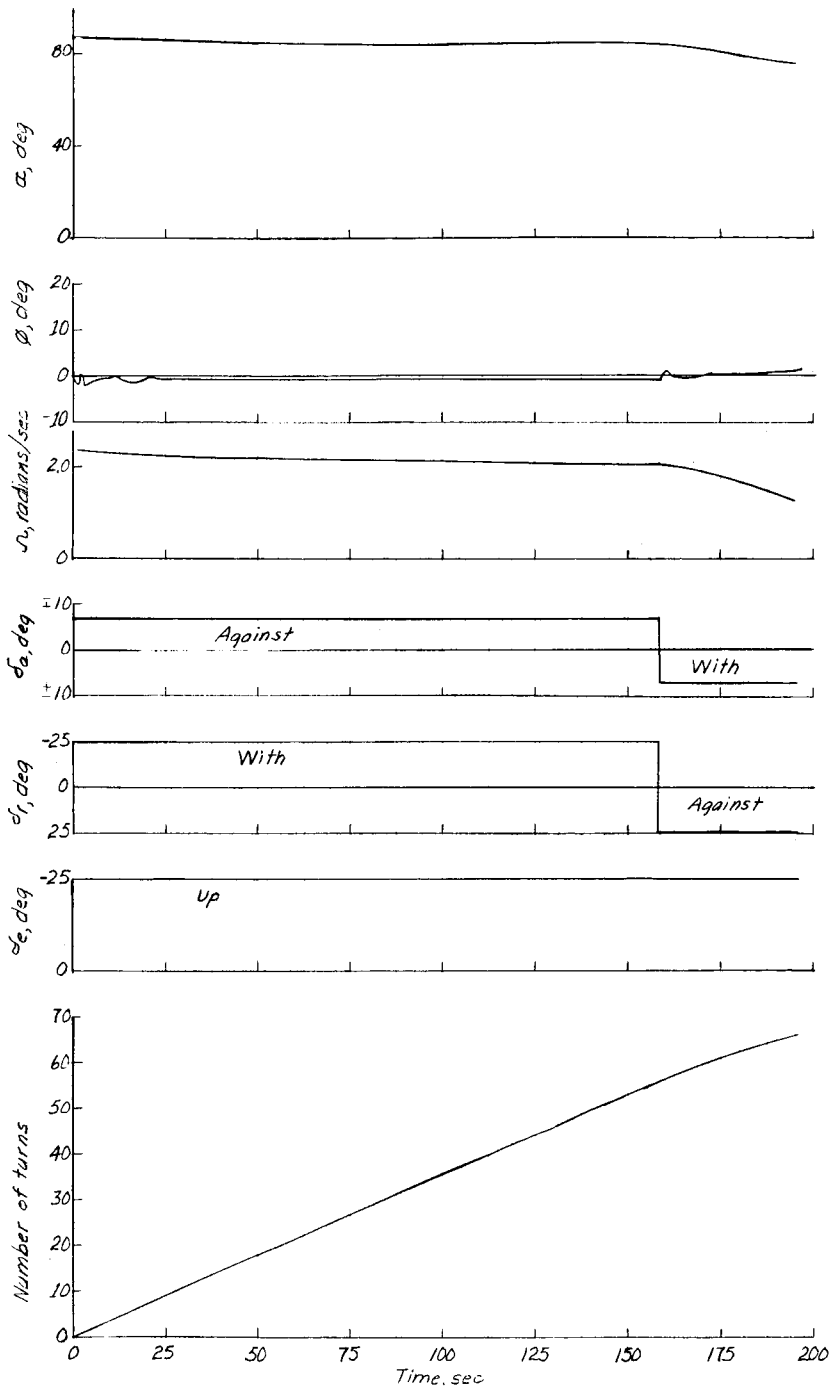

(b) Simulated model launching technique.

Figure 16.- Concluded.

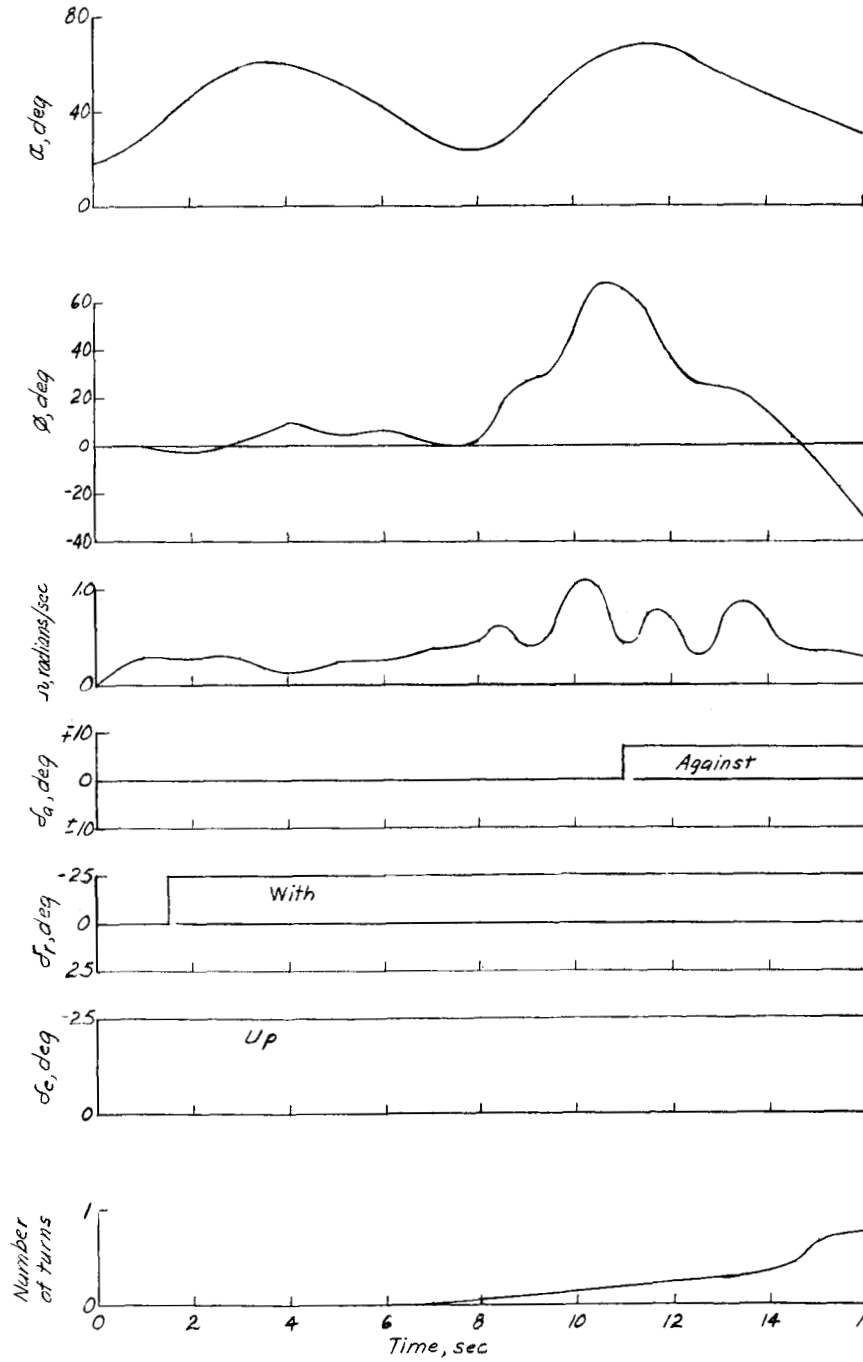

(a) Attempted spin entry from trimmed flight.

Figure 17.- Calculated spins and recoveries with use of C_{n_r} variation 1.

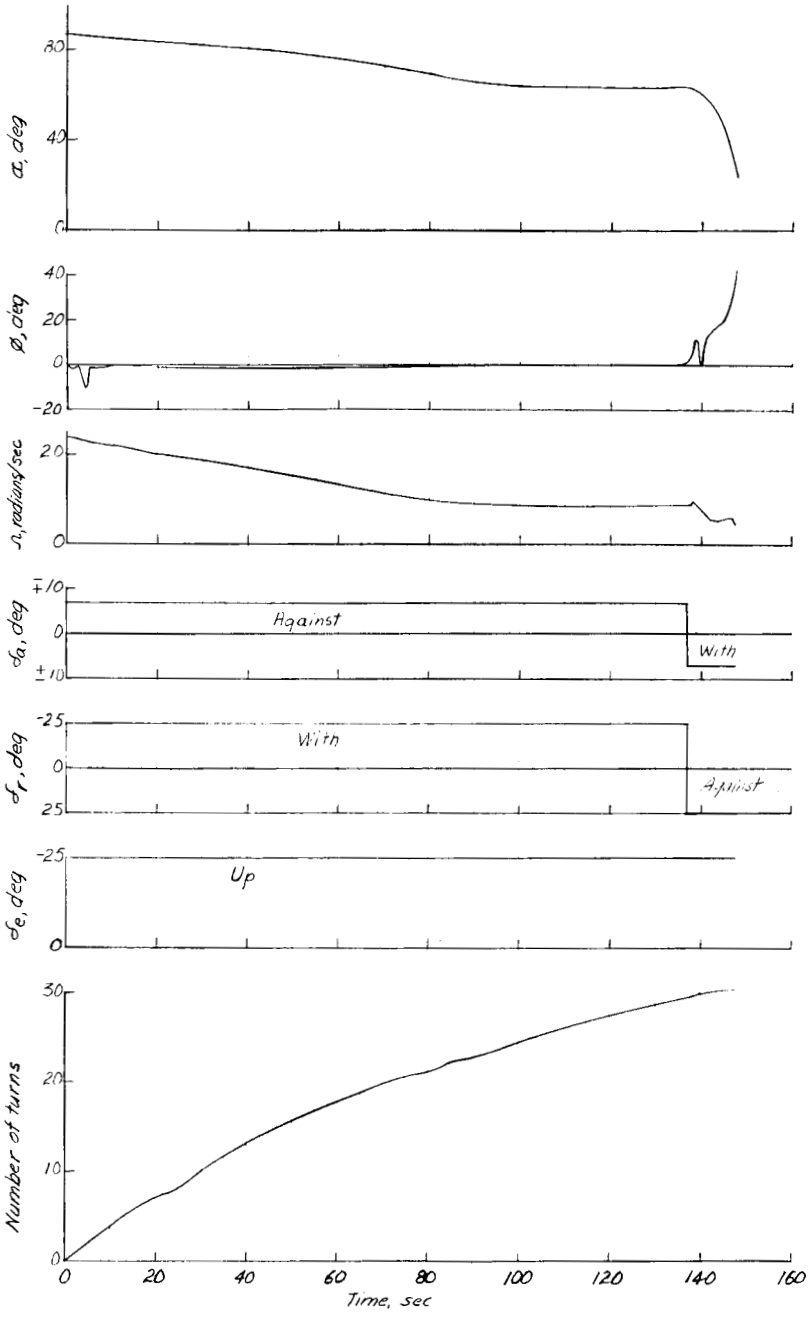

(b) Simulated model launching technique.

Figure 17.- Concluded.

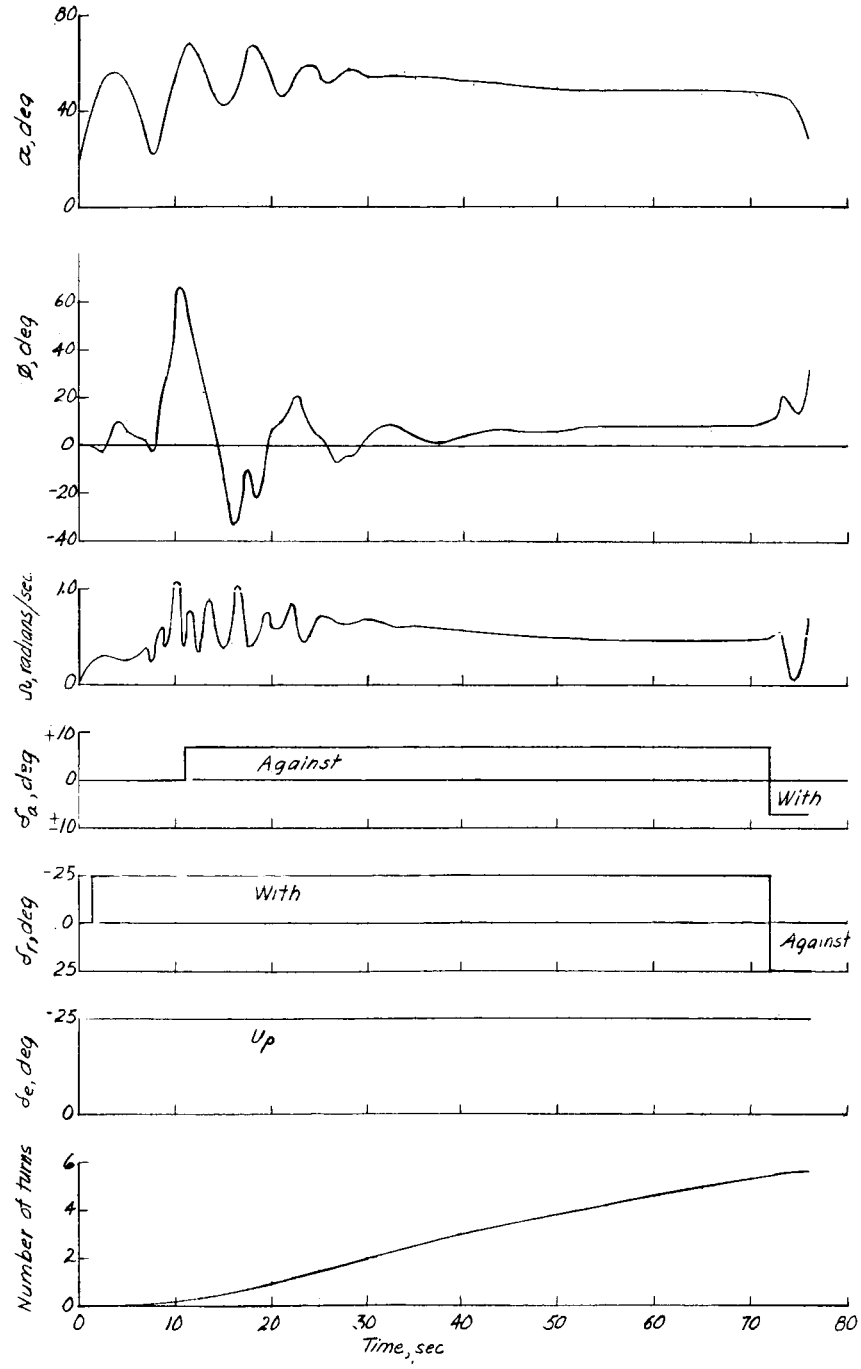

(a) Spin entry from trimmed flight.

Figure 18.- Calculated spins and recoveries with use of C_{n_r} variation 3.

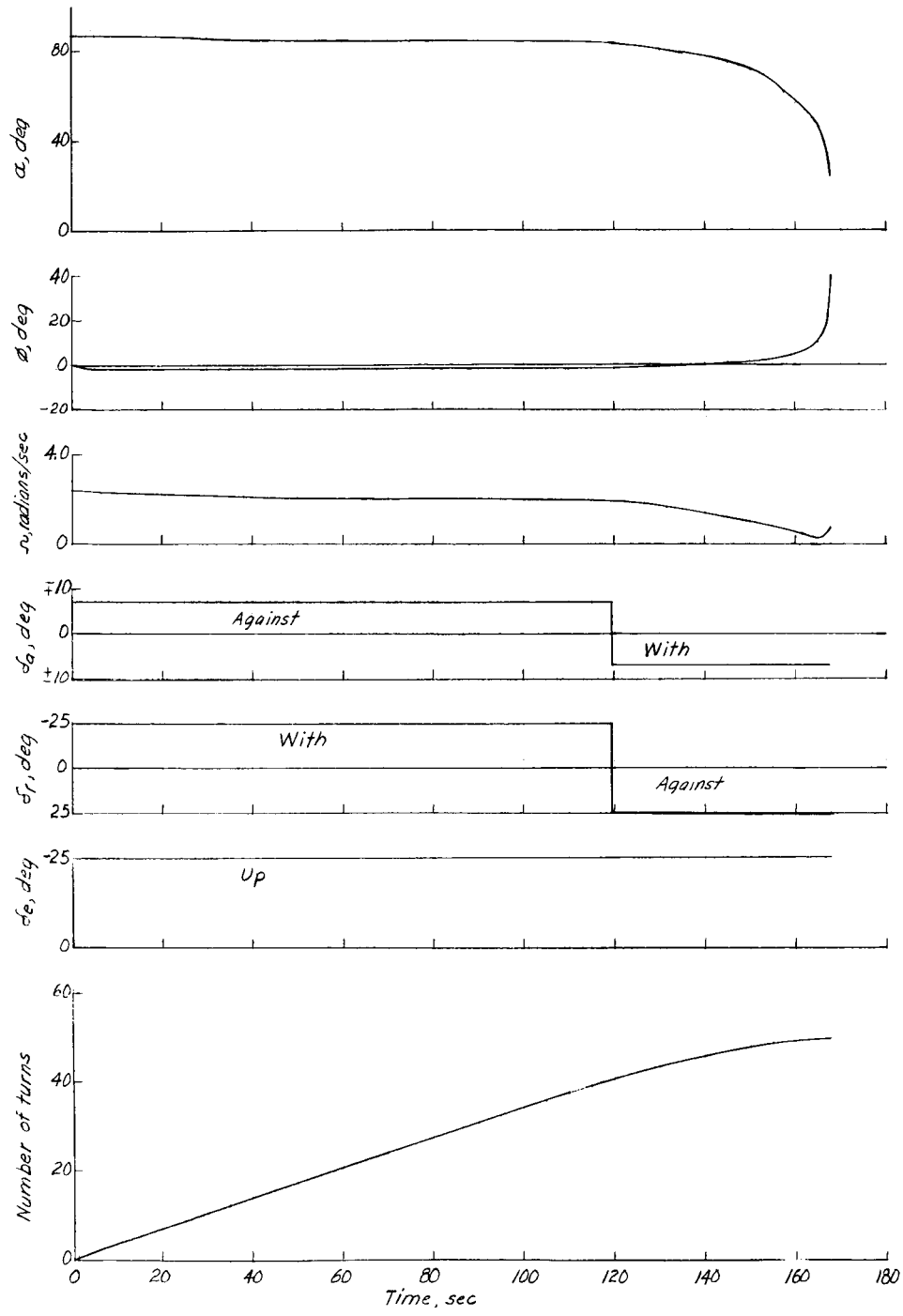

(b) Simulated model launching technique.

Figure 18.- Concluded.